haematologica
Journal of the Ferrata Storti Foundation

Lymphoma cell-driven IL-16 is expressed in activated B-cell-like diffuse large B-cell lymphomas and regulates the pro-tumor microenvironment

by Xuwen Guan, Yi Wang, Teng Fang, Jingya Wang, Ru Li, Mu Hao, and Lugui Qiu.

Received: February 26, 2024.
Accepted: September 19, 2024.

Citation: Xuwen Guan, Yi Wang, Teng Fang, Jingya Wang, Ru Li, Mu Hao, and Lugui Qiu. Lymphoma cell-driven IL-16 is expressed in activated B-cell-like diffuse large B-cell lymphomas and regulates the pro-tumor microenvironment. Haematologica. 2024 Sept 26. doi: 10.3324/haematol.2024.285304 [Epub ahead of print]

Lymphoma cell-driven IL-16 is expressed in activated B-cell-like diffuse large B-cell lymphomas and regulates the pro-tumor microenvironment

Xuwen Guan[1,2,3,4*], Yi Wang[1,2*], Teng Fang[1,2], Jingya Wang[5], Ru Li[1,2], Mu Hao[1,2#], and Lugui Qiu[1,2#]

XG and YW contributed equally as co-first authors.

[1]State Key Laboratory of Experimental Hematology, National Clinical Research Center for Blood Diseases, Haihe Laboratory of Cell Ecosystem, Institute of Hematology and Blood Diseases Hospital, Chinese Academy of Medical Sciences and Peking Union Medical College, Tianjin 300020, China.

[2]Tianjin Institutes of Health Science, Tianjin 301600, China.

[3]Department of Hematology, Tianjin First Central Hospital, Tianjin, 300192, China.

[4]Department of Hematology, Nankai University Affiliated First Central Hospital, Tianjin, 300192, China.

[5]Tianjin Medical University Cancer Institute & Hospital, National Clinical Research Center for Cancer, PR China; Key Laboratory of Cancer Prevention and Therapy, Tianjin, PR China; Tianjin's Clinical Research Center for Cancer, PR China; Department of Thoracic Oncology, Tianjin Lung Cancer Center, Tianjin Cancer Institute & Hospital, Tianjin Medical University, Tianjin, 300060, PR China.

Running heads: The role of IL-16 in DLBCL

Corresponding author: Lugui Qiu, E-mail: qiulg@ihcams.ac.cn; Mu Hao, E-mail: haomu@ihcams.ac.cn

Data-sharing statement: The data that support the findings of this study are available from the corresponding author upon reasonable request.

Word could: abstract 200; the main text 3961

Acknowledgments: We are grateful to the healthy volunteers for participation in our study. We are also grateful to ImmuneOnco Biotech (Shanghai, China) who supported IMM0306.

Funding: This investigation was supported by CAMS Innovation Fund for Medical Sciences (CIFMS) (2023-I2M-2-007) to LQ, National Natural Science Foundation of China (82341211) to LQ, National Natural Science Foundation of China (82170194, 82370210) to MH, National Natural Science Foundation of China (82000208) to XG, National Natural Science Foundation of China (82203628) to JW, Tianjin Health Research Project (TJWJ2023QN027) to XG.

Competing Interests:

The authors have declared that no conflict of interest exists.

Authors' contributions:

XG conceived and designed the project, performed experiments, analyzed data, and wrote the paper; YW performed the animal work, ELISA and collected clinical data of patients; JW performed the IHF and IHC; RL. cultured the cell lines; TF, LQ and MH analyzed the results and critically revised the manuscript; All authors provided critical review and revisions and approved the final version of the manuscript.

Abstract

The activated B-cell–like subtype of diffuse large B-cell lymphoma (ABC-DLBCL) displays a worse outcome than the germinal center B-cell–like subtype (GCB-DLBCL). Currently, targeting tumor microenvironment (TME) is the promising approach to cure DLBCL with profound molecular heterogeneity, however, the factors affecting the tumor-promoting TME of ABC-DLBCL are elusive. Here, cytokine interleukin-16 (IL-16) is expressed in tumor cells of ABC-DLBCL and secreted by the cleavage of active caspase-3. The serum IL-16 levels are not only a sensitive marker of treatment response but also positively correlated with unfavorable prognosis in DLBCL patients. While IL-16 shows few direct promotional effects on tumor cell growth *in vitro*, its bioactive form significantly promotes tumor progression *in vivo*. Mechanically, IL-16 increases the infiltration of macrophages by the chemotaxis of $CD4^+$ monocytes in the TME enhancing angiogenesis, and the expression of cytokine IL-6 and IL-10, as well as decreasing T cell infiltration to accelerate tumor progression. This study demonstrates that IL-16 exerts a novel role in coordinating the bidirectional interactions between tumor progression and the TME. IMM0306, a fusion protein of CD20 mAb with the CD47 binding domain of SIRPα, reverses the tumor-promoting effects of IL-16 ,which provides new insight into treatment strategy in ABC-DLBCL.

Introduction

DLBCL, which develops from mature B-cells, represents the most common type of non-Hodgkin lymphoma. Currently, DLBCL is mainly classified as two distinct molecular subtypes based on cell-of-origin (COO), the GCB subtypes and ABC subtypes; 10 to 15% of cases are unclassifiable[1]. It has become increasingly evident that the elements of the TME favor cancer pathogenesis and progression, and the characteristics of the TME vary in different DLBCL subtypes[2-4]. For example, ABC-DLBCL compared with GCB-DLBCL had higher macrophage[5], and $CD163^{+}$ tumor associated macrophages (M2-like) contributed poorest clinical outcome in ABC-DLBCL but not GBC DLBC[3]. Notably, the ABC-DLBCL is associated with a worse prognosis and is more aggressive than the GCB-DLBCL[6]. Therefore, distinct TMEs may confer different progression advantages on DLBCL[3].

The integration of Rituximab immunotherapy into CHOP chemotherapy for DLBCL treatment has markedly improved patient outcomes and cured over 60% of patients with DLBCL[1,6,7]. Additionally, findings of pivotal clinical trials have presented anti-CD19 Chimeric Antigen Receptor T-cell (CAR T-cell) therapy as a breakthrough in the treatment of relapsed or refractory (R/R) DLBCL[8,9]. These successes observed with both immunotherapies suggest, in part, that TME is a key target for the treatment of DLBCL. However, ~40% of patients remain insensitive to these existing treatments, Therefore, exploring the confounding factors that determine the evolution of TME in the progression of DLBCL, especially the ABC subtype, may improve the DLBCL management.

Cytokines play an important role in linking tumor cells to the TME[10]. Recent studies have shown that cytokines contribute to the growth of ABC-DLBCL[11-13]. High-throughput RNA sequencing data show that IL-16 is higher in ABC-DLBCL than GCB-DLBCL, as it is one of the transcripts belonging to multiple COO-related expression signatures to, indeed, distinguish ABC from GCB

DLBCL[14,15]. The human IL-16 gene encodes a 631-amino acid precursor IL-16 (pre-IL-16) protein, and pre-IL-16 can be cleaved by active caspase-3 into C-terminal mature IL-16 via the cleavage sites (Asp510)[16]. Mature IL-16 is generally characterized as a chemoattractant for $CD4^+$ immune cells, including T cells, mononuclear phagocytes (monocytes, macrophages, and dendritic cells), and mast cells[17-23]. Studies showed that IL-16 is expressed and released by B-cells and other immune cells (such as T cells, eosinophils and dendritic cells)[17,24-26]. However, its role in many B cell malignancies, especially in DLBCL has not yet been sufficiently studied[27,28].

In this study, we aimed to investigate the distinct pattern of IL-16 expression in the normal lymph node and DLBCL, and specifically to explore its contribution to the bidirectional interactions between tumor progression. Our findings demonstrated that the IL-16, a non-canonical cytokine expressed highly in ABC-DLBCL, was cleaved and secreted by active caspase-3. The serum IL-16 levels could be used as a sensitive marker of treatment response and poor prognosis in DLBCL. Additionally, the bioactive IL-16 driven strengthened the progression of DLBCL through regulating the macrophages enrichment which provided new insight into the personalized treatment strategy of ABC-DLBCL.

Methods

Reagents or resources

All the key reagents or resources were provided in Supplemental Tables 1

Mice Models

Six-week-old female BALB/c nude mice (Absence of thymus, absence of T-cells), BALB/c mice (immunocompetent), and NOD SCID mice (T and B lymphocyte dysfunction, low NK cell and complement binding capacity) (Beijing Vital River Laboratory Animal Technology Co., Ltd.) were

used in this study. Mice were randomly assigned to treatment groups before the start of each experiment. The investigators were not blinded during the collection or analysis of data.

Study approval

Serum samples were obtained from 87 DLBCL patients, and 10 health donors. Peripheral blood was obtained from healthy donors. Clinical information of DLBCL patients has been provided in Supplemental Tables 2. Biopsy specimens were obtained from 2 DLBCL patients. Written informed consent was obtained from all participants and this study was approved by the ethics committee of the Institute of Hematology & Blood Diseases Hospital, Tianjin, China (Approval number KT2020031-ER-2).

Commercial tissue microarrays (TMAs) with 15 tonsil tissue and 70 DLBCL tissues were purchased from Shanghai Outdo Biotech Company Co., Ltd. (HLymB085PT01, Shanghai, China). Further, this study was approved by the ethics committee of Shanghai Outdo Biotech Company Co., Ltd. (Approval number SHYJS-CP-1910014).

For animal studies, ethical approval was obtained from the ethics committee of the Institute of Hematology & Blood Diseases Hospital, Tianjin, China (Approval number KT2020031-ER-2).

For Mice models, Cell lines culture, Public databases and bioinformatics, Plasmid construction, virus production, and transduction, IHC, IHF, mIHC etc. see Supplementary methods.

Results

IL-16 expression in lymph node B-cells.

The IL-16 is abundant in immune cells[17,24-26]. Initially, we examined the expression and distribution of IL-16 in human tonsillar lymph nodes (n=15) by multi-immunofluorescence staining (mIHC) and found that IL-16-positive cells were mainly distributed in $CD20^+$ B cells (Supplementary Fig

1A-B). We next assessed the expression and distribution of IL-16 in B cells enriched germinal centers. The result showed that most of the B cells located in the mantle zone expressed IL-16, and a few B cells located in the light and dark zone expressed IL-16, suggesting that IL-16 is differentially expressed in different types of B cells (Figure 1A-B). We then confirmed these by performing conventional IHC (Supplementary Fig 1C). Further, we found IL-16 was highly abundant in Naïve B-cells (NB), Memory B-cells (MB), and plasma cells (PC) (non-light/dark areas) and relatively low in germinal center centroblasts (CB) and centrocytes (CC) (light/dark areas) (Figure 1C). Because BCL-6 is a key transcriptional repressor that regulates germinal centre B cell differentiation and may repress the expression of IL-16 in germinal center B cells[29], we analysed the expression of BCL-6. In an inverse trend to IL-16, BCL-6 expression was perfectly observed in CB and CC but not in NB, MB, and PC (Figure 1D). These findings showed that IL-16 was expressed differentially in mature B cells, and its expression in B cells could be regulated by BCL-6.

IL-16 is highly expressed in ABC-DLBCL or non-GCB-DLBCL.

DLBCL originates from mature B cells at different stages of differentiation[1]. The GCB-DLBCL originates from centrocytes, whereas the ABC-DLBCL originates from PC or MB[30]. The gene expression data of 1663 DLBCL patients (693 ABC-DLBCL and 970 GCB-DLBCL) from GEO databases were analyzed. The gene expression between the GCB-DLBCL and ABC-DLBCL groups was compared; 360 differential expression genes (DEGs) were found. Pathway enrichment analysis showed that the cytokine-cytokine receptor interaction pathway was significantly enriched in the DEGs, and IL-16 was highly expressed in ABC-DLBCL (Figure 2A, Supplementary Fig 2A).

We further confirmed whether IL-16 is differentially expressed in DLBCL in two authoritative databases with more DLBCL typing [31,32]. In particular, the highest level of IL-16 expression was found in the ABC subtype, followed by the unclassified-DLBCL, and the lowest expression was

found in the GCB subtype. Moreover, IL-16 expression was higher in N1/MCD or C1/C5 (mainly ABC-DLBCL) and lower in BN2/EZB or C4/C3 (mainly GCB-DLBCL). Consistently, we performed mIHC in DLBCL specimens (n=70) for further validation (Figure 2D). IL-16 was predominantly expressed in DLBCL tissues in tumor cells, and non-GCB-DLBCL (ABC-+ unclassified-) had a higher proportion of IL-16-positive cells compared to GCB-DLBCL (Figure 2E-H). We then confirmed these by performing conventional IHC (Supplementary Fig 2B-C). Collectively, IL-16 was expressed highly in ABC-DLBCL or non-GCB-DLBCL.

Serum IL-16 is secreted at high levels in ABC-DLBCL.

Next, we investigated the level of IL-16 in the serum of DLCBL patients (n=84) and health donors (n=10) by ELISA. Serum IL-16 levels were elevated in ABC-DLBCL, while there were no significant differences between healthy donors and GCB-DLBCL (Figure 3A, Supplementary Fig 3A). We then investigated the relationship between the IL-16 levels in DLBCL and clinical prognosis and found that high IL-16 secretion was associated with poor prognosis (OS/PFS) (Figure 3B). Consistent with previous studies, patients with ABC-DLBCL had a worse clinical prognosis compared to GCB-DLBCL patients (OS/PFS) (Supplementary Fig 3B) . To exclude interference, we verified the relationship between IL-16 levels and clinical prognosis in patients with ABC-DBCL and showed that IL-16 levels were also associated with poor prognosis (OS/PFS) (Figure 3C). In addition, IL-16 levels were correlated with IPI and treatment response, etc. (Supplementary Fig 3C-D). Moreover, IL-16 levels were positively correlated with LDH and B2M, suggesting an association between IL-16 and tumor burden (Figure 2D). We then explored whether IL-16 levels varied with changes in tumor burden after treatment, and found that in *de novo* ABC-DLBCL patients with reduced tumor burden (CR and PR) had decreased IL-16-levels after being treated with R-CHOP like treatment, but not in patients with SD and PD (Figure 3E). Similarly, in patients with R/R ABC-DLBCL treated with CD19 CAR-T cells, IL-16 decreased when the tumor reduced,

and increased when the tumor progressed (Figure 3F). To further identify the cytokines in ABC-DLBCL that correlated with the change in tumor burden, an inflammation antibody array was used to determine the levels of cytokines in sequential serum samples collected from a patient with ABC-DLBCL. We observed that IL-16, IL-3, IL-13, IFN-γ, and MIG were significantly downregulated during disease remission. In contrast, during disease progression, an opposite trend was observed, indicating the existence of a positive correlation between these cytokines and tumor burden in ABC-DLBCL (Supplementary Fig 3E). These findings indicate that IL-16 levels are high in the serum of ABC-DLBCL patients, and IL-16 levels could be used to indicate treatment response and clinical prognosis.

Caspase-3 regulates IL-16 cleavage and secretion in DLBCL.

Recent studies indicate that full-length IL-16 (80kDa, pre-IL-16) is not secreted intracellularly and its secretion depends on the cleavage of activated caspase-3 into 20kDa mature IL-16. We then assess the underlying regulatory mechanism of IL-16 secretion in DLBCL. These results revealed that, consistent with the previous findings, the mRNA and protein expression of IL-16 was elevated in the ABC-DLBCL cell line and decreased in GCB-DLBCL. However, IL-16 at 20kDa was expressed at a low level in the DLBCL cell lines (Figure 4A, Supplementary Fig 4A). In addition, we found that DLBCL cell lines secreted lower IL-16 when untreated, suggesting that IL-16 in DLBCL secretes low levels of IL-16 *in vitro* (Supplementary Fig 4B).

To further understand whether caspase-3 is orchestrating the activation and secretion of IL-16 in DLBCL, the caspase-3 activator PAC-1 was utilized to promote the activation of caspase-3. It was revealed that PAC-1 enhanced the expression of IL-16 at 20kDa, whereas no expression of IL-16 at 20kDa was observed for the IL-16-negative Su-DHL-10 cell line despite elevating caspase-3 activation. Similarly, PAC-1 stimulated caspase-3 activation and 20kDa IL-16 expression in murine

DLBCL cell line A20. Subsequently, we also found that PAC-1 contributed to IL-16 secretion (Figure 4B-C). A dose of PAC-1 (10μM) capable of inducing IL-16 secretion promoted apoptosis in less than 20% of ABC-DLBCL cells (Supplementary Fig 4C). Therefore, caspase-3 is critical for promoting IL-16 activation and secretion in DLBCL, and the reason for the low IL-16 secretion *in vitro* is that caspase-3 is barely activated *in vitro* (Supplementary Fig 2D).

We then investigated the *in vivo* role of IL-16 activation and secretion in BALB/c mice with injecting murine DLBCL cell line A20 subcutaneously (Figure 4D). Tumor volume and IL-16 secretion were positively correlated, with 20kDa IL-16 and activated caspase-3 being expressed in tumor tissue and having higher expression in larger tumors (3 weeks vs. 4 weeks) (Figure 4D-E, Supplementary Fig 4E). Notably, 20kDa IL-16 and activated caspase-3 were positively correlated (Figure 4F). Thus, *in vivo*, tumor tissues expressed activated caspase-3 and 20kDa IL-16, and secreted IL-16. These results underscore the IL-16 secretion in DLBCL is regulated by caspase-3 and is tumor-tissue-dependent.

IL-16 promotes tumor growth *in vivo*.

To the best of our knowledge, there are no relevant studies on its effect on the tumor cells of DLBCL. To accomplish this, we generated lentivirus infection with stable overexpression of IL-$16^{\triangle 511\text{-}631aa}$ (labeled with IL-$16^{\triangle}$) or EV in ABC-DLBCL cell lines (U-2932 and TMD-8) and verified its overexpression by Western blotting and ELISA (Figure 5A). Cell proliferation was detected by CCK8 assay, and essentially no effect was found on the growth of the tumor cells themselves *in vitro* (Supplementary Fig 5A). Overexpression of IL-$16^{\triangle 511\text{-}631aa}$ also did not affect the cell cycle, apoptosis in these cells, or the response of these cells to Vincristine, Doxorubicin, and 4-OOH-CY *in vitro* (Supplementary Fig 5B-D). Similarly, recombinant human IL-16 (rh-IL-16) had no significant effect on the proliferation of primary cells from DLBCL tissues and DLBCL cell

lines (Supplementary Fig 5E). Stable downexpression of pre-IL-16 (80kDa) in ABC-DLBCL cell lines (U-2932 and TMD-8) also did not affect on cell growth, cell cycle, or apoptosis in these cells, or the response of these cells to the tested drugs *in vitro* (Supplementary Fig 6A-E). Further, bulk RNA-seq data showed that pre-IL-16 downexpression had minimal effect on the gene expression in ABC-DLBCL cell lines (U-2932 and TMD-8) (Supplementary Fig 6F). Further, stable overexpression of pre-IL-16 (80kDa) also had no significant effect on cell growth *in vitro* (Supplementary Fig 6G-H). Studies have shown that IL-16 can directly promote the growth of myeloma cells with the help of CD4 or CD9 receptors [28]. However, the expression of CD4 or CD9 on the cell surface of ABC-DLBCL cells (OCI-Ly3, U-2932, and TMD-8) was low, but the expression of CD9 on the cell surface of myeloma cells (RPMI-8226) was high (Supplementary Fig 6I).

Unexpectedly, *in vivo* NOD SCID mice (T-cell deficiency) inoculated with stable overexpression of IL-16$^{\triangle 511\text{-}631aa}$ U-2932 cells exhibited apparent promotion of tumor growth (Figure 5B-C). The same experiments were validated with murine DLBCL cell line A20. We generated lentivirus infection with stable overexpression of murine IL-16$^{\triangle 507\text{-}624aa}$ (labeled with IL-16$^{\triangle}$) or EV in A20 cell lines and verified its overexpression by Western blotting and ELISA (Figure 5D). It was found that IL-16 at 20kDa did not affect the growth of tumor cells *in vitro* (Supplementary Fig 7A), but significantly promoted tumor growth in both immunodeficient BALB/c nude mice (T-cell deficiency) (Supplementary Fig 7B-D) and immunocompetent BALB/C mice (Figure 5E-F). It is suggested that IL-16 has no marked tumor-promoting effect on tumor cells themselves, but may contribute to tumor growth indirectly through other potential mechanisms.

IL-16 promotes tumor growth dependent on macrophages *in vivo*.

In order to understand how IL-16 is orchestrating the changes within the tumor microenvironments and inflammation of immune cells (such as Dendritic cells, plasmacytoid

, Neutrophils, NK cells, T cells, and Macrophages), we performed immunostaining in the immunodeficient BALB/c nude mice with A20-tumor-burden between different groups (murine IL-$16^{\Delta 507\text{-}624aa}$ overexpression vs EV) (Supplementary Fig 8A-B). The marker of macrophages F4/80 displayed a notable increase in the overexpression group (Supplementary Fig 8A). Similar results could be expected in human-derived U-2932 cells induced in NOD SCID mice (Supplementary Fig 8C) and murine-derived A20 cells induced in BALB/c mice (Figure 6A). Further, our results of mIHC results in DLBCL specimens (n=70) showed that there was a significant positive correlation between the proportion of IL-$16^{+}CD20^{+}$ cells in tumour cells and the proportion of $CD68^{+}$ macrophages in non-tumour cells (Figure 2D, Supplementary Fig 8D). These results show that IL-16 promotes macrophage infiltration.

When the A20-tumor-burden BALB/c nude mice was treated with the macrophage scavenger Clodronate Liposomes or control (Saline), the tumor-promoting effect of IL-16 was obviously reduced after removal of mouse macrophages (Figure 6B). Reportedly, macrophages promote tumor development primarily by enhancing angiogenesis as well as the expression and secretion of cytokines, such as IL-6 (directly promoting tumor growth) and IL-10 (exerting immunosuppressive effects). Representative immunostaining for the cytokines IL-6 and IL-10, as well as angiogenesis biomarker CD31 in the sections of tumor tissues from either A20 cell line-induced BALB/c nude mice or A20 cell line-induced BALB/c mice suggesting IL-16 markedly enhanced the expression of IL-6, IL-10 and angiogenesis in the macrophage compartment whether in the presence of immunodeficiency (Figure 6C-D, Supplementary Fig 9A). We then examined the polarized form of macrophages in A20 cell line-induced BALB/c mice and showed that macrophages tended to be

M2 polarized and there were more M2 macrophages in the IL-16 overexpression group (Figure 6C-D). Lastly, but notably, representative staining for H&E and mIHC of suggesting T cell markers CD3,CD8,CD4, FOXP3, T-Bet in the sections of tumor biopsy from A20 cell line-induced BALB/c mice suggesting that IL-16 inhibited infiltration of anti-tumor T cells in immunocompetent mice (Figure 6A, Supplementary Fig 9B-D). Overall, these results suggest that IL-16 facilitates the macrophages infiltration, mainly of M2 macrophages, to promote the tumor growth.

The migration of $CD4^+$ monocytes induced by DLBCL-derived IL-16.

The macrophages of the TME are mainly derived from peripheral blood monocytes, which is regulated by chemokines. IL-16 mediates chemotaxis mainly through the CD4 receptor. To ascertain that chemotaxis of DLBCL-derived IL-16 on different types of immune cells, we collected the culture medium (CM) of indicated DLBCL cells (U-2932 and TMD-8 cells with stable overexpression of IL-$16^{\Delta 511\text{-}631aa}$ or EV) and then cell migration of peripheral blood leucocyte (PBLs) is determined. IL-16 did not affect the overall chemotaxis of leukocytes essentially (Supplementary Fig 10A). We then analyzed the composition of migrated leukocytes induced by indicated CM by flow cytometry and found that IL-16 did not statistically affect the composition of leukocytes (Supplementary Fig 10B). We then revealed that IL-16 promoted the chemotaxis of monocytes but did not affect the chemotaxis of various types of T cells (Supplementary Fig 10C-D). Since monocytes are relatively low in the proportion of leukocytes, we isolated monocytes and found that monocytes were divided into two categories, including $CD11b^+CD14^{++}$ monocytes with $CD4^+$, and $CD11b^+CD14^+$ monocytes with $CD4^-$ (Figure 7A). Results showed that IL-16 notably increased monocyte chemotaxis and mainly $CD11b^+CD14^{++}$ monocytes with $CD4^+$ (Figure 7B-C). These results suggests that DLBCL derived IL-16 significantly promotes $CD4^+$ monocyte chemotaxis, by which it promotes macrophage infiltration.

IMM0306 effectively inhibits the growth of DLBCL with high IL-16 expression

Studies showed that anti-CD47 blockade limiting tumor growth in lymphoma with increased tumor-associated macrophages[33]. Multiple therapeutic antibodies, such as rituximab and antibodies targeting CD47, target tumor cells for macrophage clearance by Antibody-dependent Cellular Phagocytosis (ADCP)[33,34], and the macrophage: tumor ratio determined the effect of ADCP[20].

IMM0306, a novel fusion protein of CD20 mAb with the CD47 binding domain of SIRPα, exerts excellent cancer killing efficacy by activating macrophages via blockade of CD47-SIRPα interaction and Fc□R engagement by simultaneously binding to CD47 and CD20 of B cells[35]. We then examined whether IMM0306 could reverse the pro-tumorigenic effects of IL-16 in ABC-DLBCL.

Given that IL-16 promoted macrophage infiltration in DLBCL, we first confirmed whether increasing the macrophage: tumor ratio would enhance IMM0306-induced ADCP. The ABC-DLBCL cells were co-cultured with effector cells with different ratios as indicated, and then treated the mixed cells with IMM0306 or IgG1 mAb control. IMM0306 significantly promoted ADCP and increased the effector cells/tumor cells ratio further increasing the efficacy of IMM0306 (Figure 8A). Next, IMM0306 was used to treating ABC-DLBCL *in vivo*. Pre-IL-16 was overexpressed in the U2932 cell line via lentivirus infection (Supplementary Fig 6G) and NOD SCID mice were subcutaneously inoculated with indicated tumor cells. Mice were treated with IMM0306 and placebo respectively. Consistently, pre-IL-16 significantly promoted tumor growth in the placebo group. However, IMM0306 had a better therapeutic effect in the pre-IL-16 overexpression group than in the placebo group (Figure 8B-D). This preliminary preclinical study suggests that IMM0306 has promising antitumor effects in ABC-DLBCL with high IL-16 expression.

Discussion

In this study, we found that IL-16 was differentially expressed in different mature B cells. IL-16 was identified to be expressed in the tumor cells of ABC-DLBCL. The serum of ABC-DLBCL patients had elevated IL-16, which could predict the clinical prognosis and response to treatment. IL-16 secretion was tumor-tissue-dependent, and which could promote the tumor growth through increasing the macrophages enrichment in the TME. Lastly, IL-16 specifically induced $CD4^+$ monocyte chemotaxis, that promotes macrophage infiltration. IMM0306, which exerts cancer killing efficacy by activating macrophages, was a novel treatment approach in ABC-DLBCL.

Most DLBCL can be classified as two distinct molecular subtypes based on COO[1]. Notably, the ABC-DLBCL is more aggressive and associated with a worse prognosis than the GCB-DLBCL[6]. The new classifications based on transcriptional and mutational signatures, somatic copy number alterations, and structural variants have distinguished up to four distinct subtypes (MCD, BN2, N1, and EZB) or five clusters (termed C1- C5)[31,32]. In this study, IL-16 was found to be highly expressed in ABC-DLBCL or ABC-DLBCL-enriched N1/MCD or C1/C5 subtype. Studies demonstrated that ABC-DLBCL develops from GC B cells undergoing plasmablast or memory cell differentiation, while GCB-DLBCL develops from GC light zone B cells[30,36-38]. And our study showed that IL-16 was more abundant in plasma cells and memory cell but not GC light zone B cells, that suggesting DLBCL expressing different levels of IL-16 attributed to its being a B-cells differentiation-relative gene.

Presently, the metabolic tumor volume (MTV) calculated by FDG-PET/CT parameters and circulating tumor DNA (ctDNA) are relatively reliable strategies to assess the tumor burden and therapeutic response in DLBCL patients[39,40]. In this study, we found IL-16 was detectable in the serum of patients with ABC-DLBCL, and as a non-invasive biomarker, serum IL-16 levels can function as effective adverse prognostic factors. We observed that dynamic change of serum IL-16 levels could predict the treatment response in patients with DLBCL who receives R-CHOP or anti-

CD19 CAR T cells treatment. Next, we will also compare its accuracy and usefulness with MTV and ctDNA in the patients ABC-DLBCL.

IL-16 is not a typical cytokine that is directly secreted from cells, the secretion of which depends active caspase-3[16 41]. In this study, IL-16 secretion in DLBCL was regulated by caspase-3 which was tumor-tissue-dependent. Few previous studies have explored the role and mechanisms of IL-16 in DLBCL. In this study, we found IL-16 did not affect DLBCL cell growth *in vitro*, but its secretion accelerates tumor growth in both immunodeficient and immunologically-competent mouse models. Mechanically, IL-16 was found to increasing the infiltration of macrophages and triggered the angiogenesis, IL-6 and IL-10 expression, and decrease the infiltration of T cells in tumor tissues [42]. Macrophage clearance could reduce the tumor-promoting effect of IL-16. Moreover, DLBCL derived IL-16 significantly promotes $CD4^+$ monocyte chemotaxis, by which it promotes macrophage infiltration. Two recent pivotal studies distinguish four subtypes of the DLBCL microenvironment (GC-like, mesenchymal, inflammatory, and depleted), or nine lymphoma ecotypes (LE1-LE9) based on the transcriptional footprint of microenvironment cells or single-cell RNA-sequencing (scRNA-seq). Macrophages was abundant in inflammatory, LE1, LE4 subtypes which contain a higher proportion of ABC-DLBC[3,43]. Study demonstrated that ABC-DLBCL compared with GCB-DLBCL had higher macrophage[5], and infiltration of macrophages in the TME is associated with poor prognosis and correlates with chemotherapy resistance in most cancers[44]. Our study suggested that IL-16 was a key factor regulating the tumor microenvironment in ABC-DLBCL.

Tumor-associated macrophages facilitate tumor progression in most cancer, and therefore therapies targeting macrophages have been a topic of current studies [44]. The macrophage-dependent ADCP is the principal cytotoxic mechanism for Rituximab[34], and the proportion of macrophages determined the effect of ADCP[20]. In this study, we hypothesized that activating IL-16-recruited macrophages

might reverse its pro-tumorigenic effects. IMM0306 is a novel fusion protein of CD20 mAb with the CD47 binding domain of SIRPα, exerts cancer killing efficacy by activating macrophages[35]. In this study, IMM0306 had an excellent therapeutic effect in ABC-DLBCL with high IL-16 expression. Both in the preclinical study and a pivotal clinical trial, the combinations of anti-CD47 antibody and anti-CD20 antibody augmented the macrophage-dependent ADCP effect in DLBCL, particularly in ABC-DLBCL[45,46]. A clinical trial is being designed to evaluate the potential for clinical applications of IMM0306 in ABC-DLBCL.

In conclusion, our study shows that IL-16 promote the tumor growth by coordinating the cross-communications between the lymphoma cells and TME *in vivo*, which further suggested that IL-16 is responsible for the progression of ABC-DLBCL as a source of non-oncogene addiction is responsible for the progression of ABC-DLBCL. Therefore, targeting the pro-tumor mechanisms of IL-16 could provide an attractive biology-driven personalized treatment strategy for therapeutic vulnerability in ABC-DLBCL.

References

1. Sehn LH, Salles G. Diffuse Large B-Cell Lymphoma. N Engl J Med. 2021;384(9):842-858.
2. Scott DW, Gascoyne RD. The tumour microenvironment in B cell lymphomas. Nat Rev Cancer. 2014;14(8):517-534.
3. Kotlov N, Bagaev A, Revuelta MV, et al. Clinical and biological subtypes of B-cell lymphoma revealed by microenvironmental signatures. Cancer Discov. 2021;1(6):1468-1489.
4. Riihijarvi S, Fiskvik I, Taskinen M, et al. Prognostic influence of macrophages in patients with diffuse large B-cell lymphoma: a correlative study from a Nordic phase II trial. Haematologica. 2015;100(2):238-245.
5. Xu-Monette ZY, Xiao M, Au Q, et al. Immune Profiling and Quantitative Analysis Decipher the Clinical Role of Immune-Checkpoint Expression in the Tumor Immune Microenvironment of DLBCL. Cancer Immunol Res. 2019;7(4):644-657.
6. Bakhshi TJ, Georgel PT. Genetic and epigenetic determinants of diffuse large B-cell lymphoma. Blood Cancer J. 2020;10(12):123.
7. Flowers CR, Sinha R, Vose JM. Improving outcomes for patients with diffuse large B-cell lymphoma. CA Cancer J Clin. 2010;60(6):393-408.
8. Abramson JS, Palomba ML, Gordon LI, et al. Lisocabtagene maraleucel for patients with relapsed or refractory large B-cell lymphomas (TRANSCEND NHL 001): a multicentre seamless design study. Lancet. 2020;396(10254):839-852.
9. Neelapu SS, Locke FL, Bartlett NL, et al. Axicabtagene Ciloleucel CAR T-Cell Therapy in Refractory Large B-Cell Lymphoma. N Engl J Med. 2017;377(26):2531-2544.
10. Galdiero MR, Marone G, Mantovani A. Cancer Inflammation and Cytokines. Cold Spring Harb Perspect Biol. 2018;10(8):a028662.
11. Hashwah H, Bertram K, Stirm K, et al. The IL-6 signaling complex is a critical driver, negative prognostic factor, and therapeutic target in diffuse large B-cell lymphoma. EMBO Mol Med. 2019;11(10):e10576.
12. Gupta M, Han JJ, Stenson M, et al. Elevated serum IL-10 levels in diffuse large B-cell lymphoma: a mechanism of aberrant JAK2 activation. Blood. 2012;119(12):2844-2853.
13. Beguelin W, Sawh S, Chambwe N, et al. IL10 receptor is a novel therapeutic target in DLBCLs. Leukemia. 2015;29(8):1684-1694.
14. Reddy A, Zhang J, Davis NS, et al. Genetic and Functional Drivers of Diffuse Large B Cell Lymphoma. Cell. 2017;171(2):481-494.e15.
15. Wright G, Tan B, Rosenwald A, Hurt EH, Wiestner A, Staudt LM. A gene expression-based method to diagnose clinically distinct subgroups of diffuse large B cell lymphoma. Proc Natl Acad Sci U S A. 2003;100(17):9991-9996.
16. Richmond J, Tuzova M, Cruikshank W, Center D. Regulation of cellular processes by interleukin-16 in homeostasis and cancer. J Cell Physiol. 2014;229(2):139-147.
17. Kaser A, Dunzendorfer S, Offner FA, et al. B lymphocyte-derived IL-16 attracts dendritic cells and Th cells. J Immunol. 2000;165(5):2474-2480.
18. Lynch EA, Heijens CA, Horst NF, Center DM, Cruikshank WW. Cutting edge: IL-16/CD4 preferentially induces Th1 cell migration: requirement of CCR5. J Immunol. 2003;171(10):4965-4968.
19. McFadden C, Morgan R, Rahangdale S, et al. Preferential migration of T regulatory cells induced by IL-16. J Immunol. 2007;179(10):6439-6445.
20. Lossos C, Liu Y, Kolb KE, et al. Mechanisms of Lymphoma Clearance Induced by High-Dose Alkylating Agents. Cancer Discov. 2019;9(7):944-961.
21. Bernstein HB, Plasterer MC, Schiff SE, Kitchen CM, Kitchen S, Zack JA. CD4 expression on activated NK cells: ligation of CD4 induces cytokine expression and cell migration. J Immunol. 2006;177(6):3669-3676.

22. Cruikshank W, Little F. Interleukin-16: the ins and outs of regulating T-cell activation. Crit Rev Immunol. 2008;28(6):467-483.
23. Qi JC, Wang J, Mandadi S, et al. Human and mouse mast cells use the tetraspanin CD9 as an alternate interleukin-16 receptor. Blood. 2006;107(1):135-142.
24. Liu S, Lei Z, Li J, et al. Interleukin 16 contributes to gammaherpesvirus pathogenesis by inhibiting viral reactivation. PLoS Pathog. 2020;16(7):e1008701.
25. Elssner A, Doseff AI, Duncan M, Kotur M, Wewers MD. IL-16 is constitutively present in peripheral blood monocytes and spontaneously released during apoptosis. J Immunol. 2004;172(12):7721-7725.
26. Wu DM, Zhang Y, Parada NA, et al. Processing and release of IL-16 from CD4+ but not CD8+ T cells is activation dependent. J Immunol. 1999;162(3):1287-1293.
27. Bozorgmehr N, Okoye I, Oyegbami O, et al. Expanded antigen-experienced CD160(+)CD8(+)effector T cells exhibit impaired effector functions in chronic lymphocytic leukemia. J Immunother Cancer. 2021;9(4):e002189.
28. Atanackovic D, Hildebrandt Y, Templin J, et al. Role of interleukin 16 in multiple myeloma. J Natl Cancer Inst. 2012;104(13):1005-1020.
29. Basso K, Saito M, Sumazin P, et al. Integrated biochemical and computational approach identifies BCL6 direct target genes controlling multiple pathways in normal germinal center B cells. Blood. 2010;115(5):975-984.
30. Venturutti L, Melnick AM. The dangers of deja vu: memory B cells as the cells of origin of ABC-DLBCLs. Blood. 2020;136(20):2263-2274.
31. Schmitz R, Wright GW, Huang DW, et al. Genetics and Pathogenesis of Diffuse Large B-Cell Lymphoma. N Engl J Med. 2018;378(15):1396-1407.
32. Chapuy B, Stewart C, Dunford AJ, et al. Molecular subtypes of diffuse large B cell lymphoma are associated with distinct pathogenic mechanisms and outcomes. Nat Med. 2018;24(5):679-690.
33. Ennishi D, Healy S, Bashashati A, et al. TMEM30A loss-of-function mutations drive lymphomagenesis and confer therapeutically exploitable vulnerability in B-cell lymphoma. Nat Med. 2020;26(4):577-588.
34. Pinney JJ, Rivera-Escalera F, Chu CC, et al. Macrophage hypophagia as a mechanism of innate immune exhaustion in mAb-induced cell clearance. Blood. 2020;136(18):2065-2079.
35. Yu J, Li S, Chen D, et al. IMM0306, a fusion protein of CD20 mAb with the CD47 binding domain of SIRPalpha, exerts excellent cancer killing efficacy by activating both macrophages and NK cells via blockade of CD47-SIRPalpha interaction and Fc□R engagement by simultaneously binding to CD47 and CD20 of B cells. Leukemia. 2023;37(3):695-698.
36. Basso K, Dalla-Favera R. Germinal centres and B cell lymphomagenesis. Nat Rev Immunol. 2015;15(3):172-184.
37. Holmes AB, Corinaldesi C, Shen Q, et al. Single-cell analysis of germinal-center B cells informs on lymphoma cell of origin and outcome. J Exp Med. 2020;217(10):e20200483.
38. Venturutti L, Teater M, Zhai A, et al. TBL1XR1 Mutations Drive Extranodal Lymphoma by Inducing a Pro-tumorigenic Memory Fate. Cell. 2020;182(2):297-316.e27.
39. Cottereau AS, Meignan M, Nioche C, et al. Risk stratification in diffuse large B-cell lymphoma using lesion dissemination and metabolic tumor burden calculated from baseline PET/CT(dagger). Ann Oncol. 2021;32(3):404-411.
40. Rivas-Delgado A, Nadeu F, Enjuanes A, et al. Mutational Landscape and Tumor Burden Assessed by Cell-free DNA in Diffuse Large B-Cell Lymphoma in a Population-Based Study. Clin Cancer Res. 2021;27(2):513-521.
41. Cubillos-Ruiz JR, Bettigole SE, Glimcher LH. Tumorigenic and Immunosuppressive Effects of Endoplasmic Reticulum Stress in Cancer. Cell. 2017;168(4):692-706.
42. Mulder K, Patel AA, Kong WT, et al. Cross-tissue single-cell landscape of human monocytes and macrophages in health and disease. Immunity. 2021;54(8):1883-1900.e5.

43. Steen CB, Luca BA, Esfahani MS, et al. The landscape of tumor cell states and ecosystems in diffuse large B cell lymphoma. Cancer Cell. 2021;39(10):1422-1437.e10.
44. Cassetta L, Pollard JW. Targeting macrophages: therapeutic approaches in cancer. Nat Rev Drug Discov. 2018;17(12):887-904.
45. Advani R, Flinn I, Popplewell L, et al. CD47 Blockade by Hu5F9-G4 and Rituximab in Non-Hodgkin's Lymphoma. N Engl J Med. 2018;379(18):1711-1721.
46. Chao MP, Alizadeh AA, Tang C, et al. Anti-CD47 antibody synergizes with rituximab to promote phagocytosis and eradicate non-Hodgkin lymphoma. Cell. 2010;142(5):699-713.

Fig.1 IL-16 expression in lymph node B-cells. (A) Representative multi-immunofluorescence staining(mIHC) images for IL-16 protein expression (red pseudocolor) in the germinal center from tonsil specimens. CD20 (B cells, green pseudocolor) and DAPI nuclear stain (blue pseudocolor) included to discern tissue landscape. Scale bars apply across each row. (B) Proportion of IL-16-positive cells in different types of B cells, n=15. MZ indicated Mantle zone, D/L indicated Dark/light zone. (C-D) Expression of IL-16 and BCL-6 mRNA in mature B cells from tonsil at different stages of differentiation. NB indicated Naïve B-cells (n=5), CB indicated Germinal center centroblasts (n=14), CC indicated centrocytes (n=13), MB indicated Memory B-cells (n=5), and PC indicated plasma cells (n=5). (gene expression data was collected from GEO, GSE2350). Data shown are mean ± SD. p values are based on unpaired t-test. ns=non-significant; *p < 0.05, **p < 0.01, ***p < 0.001, ****p < 0.0001.

Fig.2 IL-16 is highly expressed in the activated B-cell–like subtype of diffuse large B-cell lymphoma (ABC-DLBCL) or the non-germinal center B-cell–like subtype of DLBCL (non-GCB-DLBCL). (A) Volcano map indicates the differentially expressed genes (DEGs) between germinal center B-cell–like subtype DLBCL (GCB-DLBCL) (n=970) and ABC-DLBCL (n=693) from 4 merged DLBCL databases (GSE10846, GSE31312, GSE87371, and GSE117556) (|FC|>1.5, FDR<0.05). The red triangle indicates IL-16 highly expressed in ABC-DLBCL. (B) Difference of IL-16 mRNA expression between different types of DLBCL (gene expression data was collected from Schimitz et al[31].). (C) Difference of IL-16 mRNA expression between different types of DLBCL (gene expression data was collected from Chapuy et al[32]). (D) Representative mIHC images for IL-16 protein expression (pink pseudocolor) in non-GCB-DLBCL and GCB-DLBCL specimens. CD20 (tumor cells, green pseudocolor), CD3 (T cells, yellow pseudocolor), CD68

(macrophages, red pseudocolor), and DAPI nuclear stain (blue pseudocolor) included to discern tissue landscape. Scale bars apply across each row. (E-F) Proportion of IL-16-positive cells in the GCB-DLBCL (n=13) or non-GCB-DLBCL (n=57) tumor cells ($CD20^+$) and different types of immune cells ($CD3^+$ T cells and $CD68^+$ macrophages). (G-F) Proportion of IL-16-positive cells or IL-16-CD20 double positive cells in the GCB-DLBCL (n=13) or non-GCB-DLBCL (n=57) specimens. Data shown are mean ± SD. p values are based on unpaired t-test. ns=non-significant; *p < 0.05, **p < 0.01, ***p < 0.001, ****p < 0.0001.

Fig.3 Serum IL-16 is secreted at high levels in ABC-DLBCL. (A) Detection of the levels of IL-16 in serum from DLCBL patients (39 GCB-DLBCL and 45 ABC-DLBCL) and health donors (n=10) by ELISA. (B-C) Overall-Survival (OS) and Progression-Free-Survival (PFS) of DLBCL patients or ABC-DLBCL patients based on the low and high levels of serum IL-16. (D) The correlations between serum IL-16 of ABC-DLBCL patients and LDH or β2M are analyzed. n=45 (E) Detection of the levels of serum IL-16 from 25 pairs of de novo DLBCL patients (before treatment and after at least 2 cycles of treatment) by ELISA. The differences in IL-16 between the two time points are analyzed. The left panel exhibits the patients who achieve Complete Response (CR) and Partial Response (PR) after treatment (n=21), and the right panel exhibits the patients who were Stable Disease (SD) and Progressive Disease (PD) after treatment (n=4). The baseline (BL) indicates the serum of patients is collected before treatment. (F) Dynamic changes of serum IL-16, IL-6 a d IL-10 in three Relapsed Refractory (R/R) ABC-DLBCL patients during the anti-CD19 CAR T cell therapy at indicated time points. CRS indicates the patients have cytokine release syndrome. Data shown are mean ± SD. p values are based on unpaired or paired t-test, Log-rank

(Mantel-Cox) test and Pearson correlation. ns=non-significant; *p < 0.05, **p < 0.01, ***p < 0.001, ****p < 0.0001.

Fig.4 Caspase-3 regulates IL-16 cleavage and secretion in DLBCL. (A) Detection of IL-16 protein expression in DLBCL cell lines (ABC-DLBCL cell lines: OCI-Ly3, U-2932, and TMD-8; GCB-DLBCL cell lines: Su-DHL-6, Su-DHL-10, and DoHH2) by western blotting. β-actin is used as a loading control. 80kDa IL-16 indicates full-length Pre-IL-16, and 20kDa IL-16 indicates cleaved mature IL-16. (B-C) Human DLBCL cell lines (OCI-Ly3, U-2932, and Su-DHL-10) and murine DLBCL cell lines (A20) are treated with indicated dose of PAC-1 for 24h, and (B) protein expression of IL-16 and Caspase-3 are determined by western blotting. β-Actin is used as a loading control. C-Caspase-3 indicated cleaved Caspase-3. (C) Secretion levels of IL-16 in the culture medium are quantified by ELISA. (D-F) The BALB/c mice were inoculated subcutaneously with A20 cells (n=4/group), the serum was collected at different time points (week0, week3 and week4), and the tumor tissues were collected at different time points (week3 and week4). (D) Detection of the levels of IL-16 in serum from mice. (E) Detection of IL-16 and Caspase-3 protein expression by western blotting in different DLBCL tissues. β-Actin is used as a loading control. (F) The correlation between the expression and C-Caspase-3 and mature IL-16. Data shown are mean ± SD. p values are based on unpaired t-test, and Pearson correlation. ns=non-significant; *p < 0.05, **p < 0.01, ***p < 0.001, ****p < 0.0001.

Fig.5 IL-16 promotes tumor growth *in vivo*. (A) Detection of IL-16 protein expression by western blotting in DLBCL cell lines (U-2932 and TMD-8) with stable overexpression of IL-16$^{\Delta 511\text{-}631aa}$ (labeled with IL-16$^{\Delta}$) or EV. β-Actin is used as a loading control. EV indicated empty vector

controls. Secretion levels of IL-16 in the culture medium of indicated DLBCL cell lines (U-2932 and TMD-8 with stable overexpression of IL-16$^{\Delta 511\text{-}631aa}$ (labeled with IL-16$^{\Delta}$) or EV, 5x10^5 cells/ml, 24h) are quantified by ELISA. (B-C) NOD SCID mice are inoculated with U-2932 cells with overexpression of IL-16$^{\Delta 511\text{-}631aa}$ (labeled with IL-16$^{\Delta}$) or EV respectively (n=5/group). Comparison volumes of tumors growing subcutaneously in mice. When tumors are palpable, tumor volumes are measured and calculated every other day. When the mice were anesthetized and sacrificed, the tumor samples were collected to measure volume. (D) Detection of mature IL-16 protein expression by western blotting in A20 cells with stable murine IL-16$^{\Delta 507\text{-}624aa}$ overexpression or EV. β-Actin is used as a loading control. EV indicated empty vector controls. Secretion levels of IL-16 in the culture medium of A20 cell lines with stable overexpression of murine IL-16$^{\Delta 507\text{-}624aa}$ or EV (5x10^5 cells/ml, 24h) are quantified by ELISA. (E-F) BALB/c mice are inoculated with A20 cells with murine IL-16$^{\Delta 507\text{-}624aa}$ overexpression or EV respectively for 15/20/25 days (n=4/group) A collection of tumors and tumor volumes from mice. Data shown are mean ± SD. p values are based on two-way ANOVA and unpaired or paired t-test. ns=non-significant; *p < 0.05, **p < 0.01, ***p < 0.001, ****p < 0.0001.

Fig.6 IL-16 promotes tumor growth dependent on macrophages *in vivo*. (A) Representative immunostaining and quantification for T cells markers CD3 and macrophage marker F4/80 in the sections of tumor tissues from BALB/c mice. The difference in the infiltration of indicated cells in tumor tissues between different groups (murine IL-16$^{\Delta 507\text{-}624aa}$ overexpression vs EV) is analyzed. Scale bars apply across each row. (B) BALB/c nude mice are inoculated with A20 cells with murine IL-16$^{\Delta 507\text{-}624aa}$ overexpression or EV respectively (n=5/group) on Day1. Mice are treated with Control (saline) or Clodronate Liposomes at indicated time points (Day0, 4, 8, 12, i.p.). When

the mice were anesthetized and sacrificed, the tumor samples were collected to measure volume. (C-D) Representative immunostaining and quantification for the cytokines IL-6 and IL-10, vascular endothelial cells marker CD31 (microvascular density), CD163 and F4/80, and CD86 and F4/80, in the sections of tumor tissues from BALB/c mice. The difference in the infiltration of indicated cells in tumor tissues between different groups (murine IL-16$^{\Delta 507\text{-}624aa}$ overexpression vs EV) is analyzed. Scale bars apply across each row. Data shown are mean ± SD. p values are based on unpaired or paired t-test. ns=non-significant; *p < 0.05, **p < 0.01, ***p < 0.001, ****p < 0.0001.

Fig.7 The migration of CD4$^+$ monocytes induced by DLBCL-derived IL-16. (A) the monocytes were isolated from healthy donors. The monocytes were stained with anti-CD11b-APC-Cy7, anti-CD14-APC, anti-CD4-FITC antibodies. (B) Cell migration of monocytes is determined by transwell assay (1h) combined with the CCK-8 test. 10% FBS culture medium were used as control. Rate of chemotaxis (%)=($OD_{Lower\ chamber}$-$OD_{Background}$/ $OD_{Upper\ chamber}$-$OD_{Background}$)x100. (C) the proportion of indicated monocytes in migrated monocytes. Data shown are mean ± SD. p values are based on unpaired t-test. ns=non-significant; *p < 0.05, **p < 0.01, ***p < 0.001, ****p < 0.0001.

Fig.8 Antitumor effects of IMM0306 in ABC-DLBCL. (A) DLBCL cells (TMD-8 and U-2932) are labeled with CellTrace™ CFSE, and effector cells (THP-1, a human macrophage/monocyte cell line) are labeled with CellTrace™ Violet. Tumor cells are co-cultured with effector cells at the indicated ratio for 30min with the 10μg/ml IMM0306 or IgG1 mAb treatment. CellTrace™ CFSE$^+$ tumor cells are selected to analyze the percentage of CellTrace™ CFSE$^+$ CellTrace™ Violet$^+$ tumor cells phagocytosed by effector cells (ADCP). (B-D) NOD SCID mice are inoculated with U-2932 cells with pre-IL-16 overexpression or EV respectively (n =5/group). When the tumors reached a

mean of 200 mm^3, mice were treated with Control (placebo: human IgG1 control, 2.5mg/kg, i.v., Day2, 4, 6, 9, 11, and 13) and IMM0306 (2.5mg/kg, i.v., Day2, 4, 6, 9, 11, and 13). The volumes of tumors of mice is measured and calculated every other day after treatment. Data shown are mean ± SD. p values are based on the two-way ANOVA and the unpaired or paired t-test. ns=non-significant; *$p < 0.05$, **$p < 0.01$, ***$p < 0.001$, ****$p < 0.0001$.

Fig.1

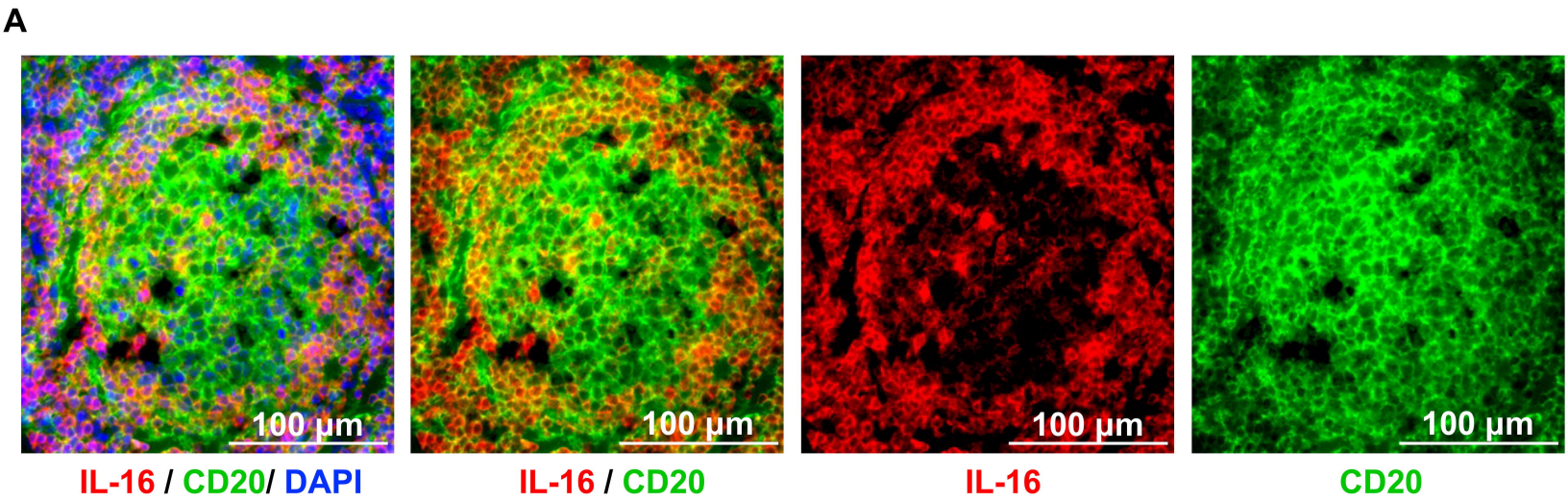
A
100 μm
100 μm
100 μm
100 μm
IL-16 / CD20/ DAPI
IL-16 / CD20
IL-16
CD20
B
% IL-16+cells in CD20+cells
MZ
D/L
Germinal center from tonsil
C
mRNA expression of IL16
NB
CB
CC
MB
PC
D
mRNA expression of BCL6
NB
CB
CC
MB
PC
Mature B cell collected from tonsil

Fig.2

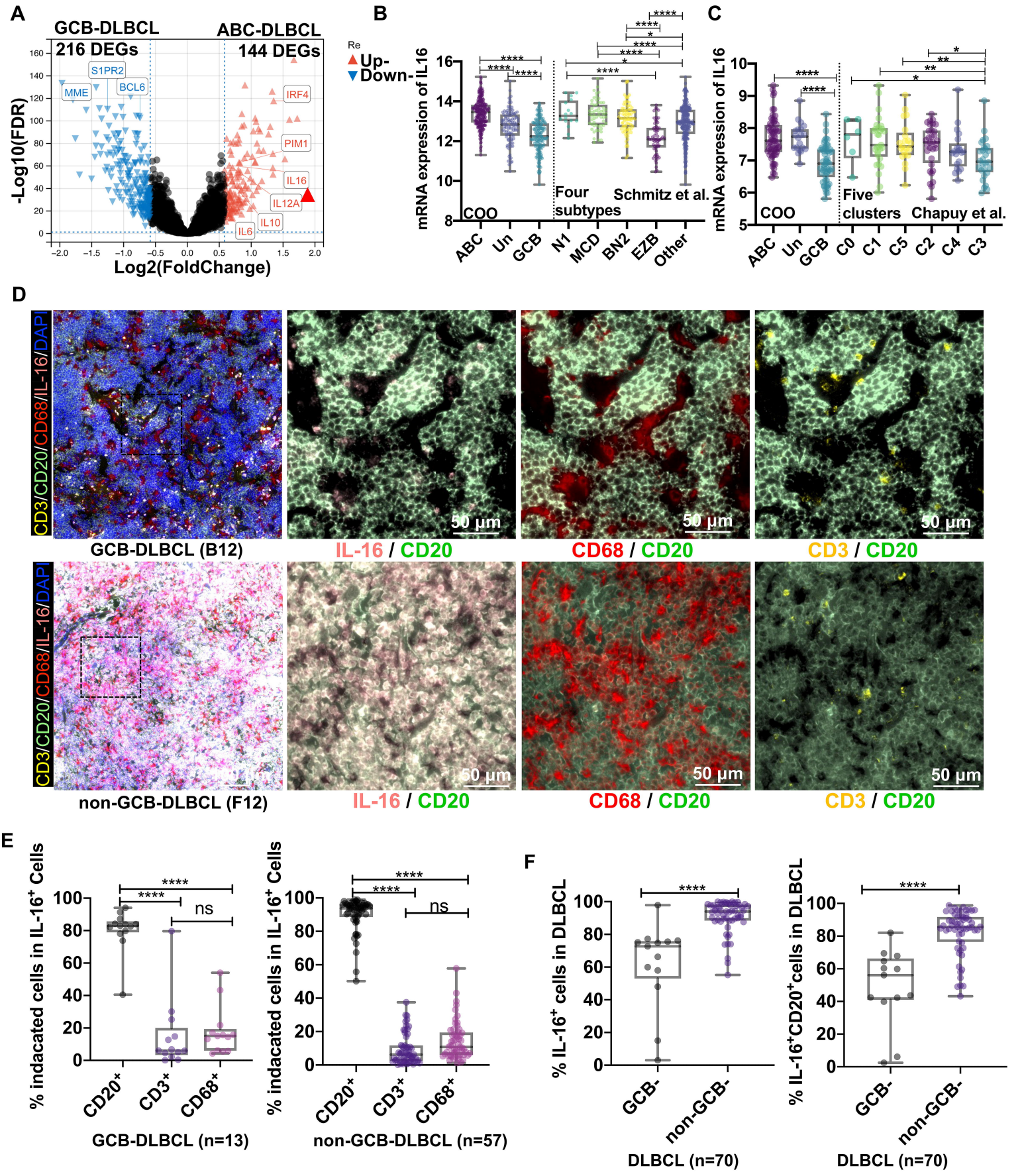
A
GCB-DLBCL
ABC-DLBCL
216 DEGs
144 DEGs
S1PR2
MME
BCL6
IRF4
PIM1
IL16
IL12A
IL10
IL6
-Log10(FDR)
Log2(FoldChange)
B
Re
Up-
Down-
mRNA expression of IL16
COO
Four subtypes
Schmitz et al.
ABC
Un
GCB
N1
MCD
BN2
EZB
Other
C
mRNA expression of IL16
COO
Five clusters
Chapuy et al.
ABC
Un
GCB
C0
C1
C5
C2
C4
C3
D
CD3/CD20/CD68/IL-16/DAPI
GCB-DLBCL (B12)
IL-16 / CD20
CD68 / CD20
CD3 / CD20
non-GCB-DLBCL (F12)
50 μm
E
% indacated cells in IL-16+ Cells
CD20+
CD3+
CD68+
ns
GCB-DLBCL (n=13)
non-GCB-DLBCL (n=57)
F
% IL-16+ cells in DLBCL
% IL-16+CD20+cells in DLBCL
GCB-
non-GCB-
DLBCL (n=70)

Fig.3

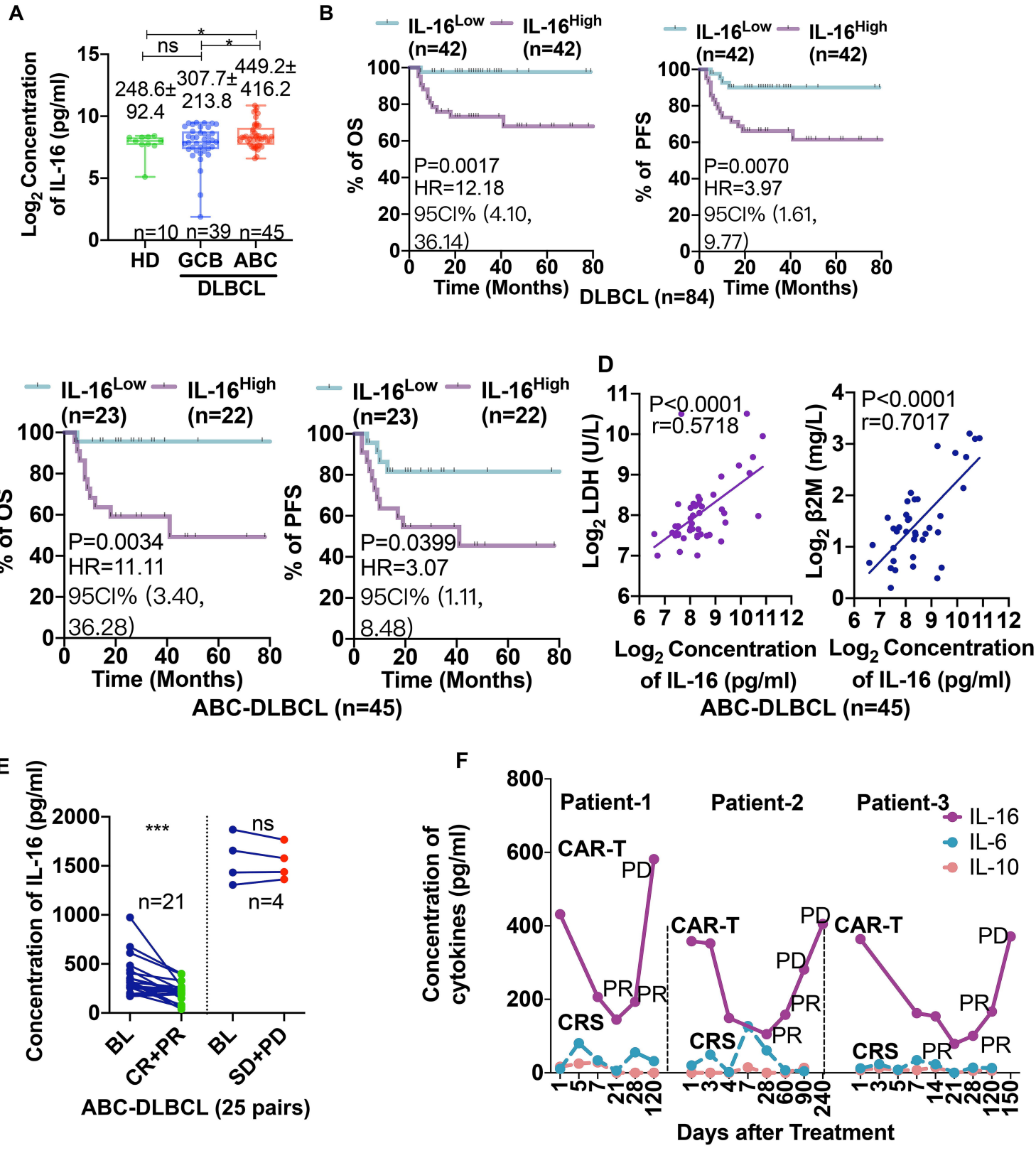
A
Log2 Concentration of IL-16 (pg/ml)
ns
*
*
248.6± 92.4
307.7± 213.8
449.2± 416.2
n=10
n=39
n=45
HD
GCB
ABC
DLBCL
B
IL-16Low (n=42)
IL-16High (n=42)
% of OS
P=0.0017
HR=12.18
95CI% (4.10, 36.14)
Time (Months)
% of PFS
P=0.0070
HR=3.97
95CI% (1.61, 9.77)
DLBCL (n=84)
C
IL-16Low (n=23)
IL-16High (n=22)
% of OS
P=0.0034
HR=11.11
95CI% (3.40, 36.28)
% of PFS
P=0.0399
HR=3.07
95CI% (1.11, 8.48)
ABC-DLBCL (n=45)
D
Log2 LDH (U/L)
P<0.0001
r=0.5718
Log2 β2M (mg/L)
P<0.0001
r=0.7017
Log2 Concentration of IL-16 (pg/ml)
ABC-DLBCL (n=45)
E
Concentration of IL-16 (pg/ml)
***
ns
n=21
n=4
BL
CR+PR
BL
SD+PD
ABC-DLBCL (25 pairs)
F
Concentration of cytokines (pg/ml)
Patient-1
Patient-2
Patient-3
IL-16
IL-6
IL-10
CAR-T
PD
PR
CRS
Days after Treatment

Fig.4

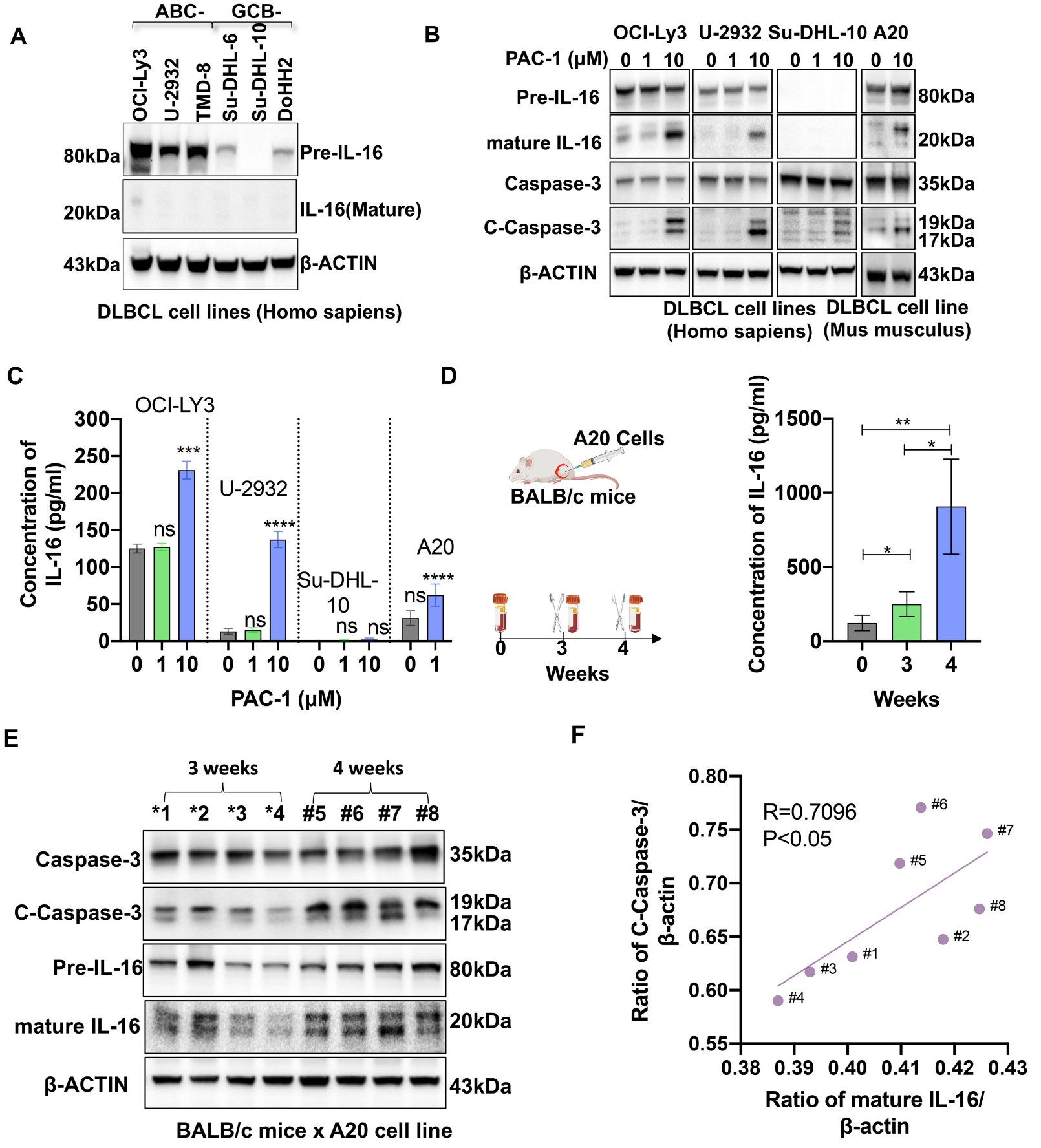
A
ABC-
GCB-
OCI-Ly3
U-2932
TMD-8
Su-DHL-6
Su-DHL-10
DoHH2
80kDa
Pre-IL-16
20kDa
IL-16(Mature)
43kDa
β-ACTIN
DLBCL cell lines (Homo sapiens)
B
OCI-Ly3 U-2932 Su-DHL-10 A20
PAC-1 (μM) 0 1 10 0 1 10 0 1 10 0 10
Pre-IL-16
mature IL-16
Caspase-3
C-Caspase-3
β-ACTIN
80kDa
20kDa
35kDa
19kDa
17kDa
43kDa
DLBCL cell lines (Homo sapiens)
DLBCL cell line (Mus musculus)
C
OCI-LY3
U-2932
Su-DHL-10
A20
Concentration of IL-16 (pg/ml)
300
250
200
150
100
50
0
***
ns
****
ns
ns
ns
****
ns
0 1 10 0 1 10 0 1 10 0 1
PAC-1 (μM)
D
A20 Cells
BALB/c mice
0
3
4
Weeks
Concentration of IL-16 (pg/ml)
1500
1000
500
0
**
*
*
0 3 4
Weeks
E
3 weeks
4 weeks
*1 *2 *3 *4 #5 #6 #7 #8
Caspase-3
C-Caspase-3
Pre-IL-16
mature IL-16
β-ACTIN
35kDa
19kDa
17kDa
80kDa
20kDa
43kDa
BALB/c mice x A20 cell line
F
R=0.7096
P<0.05
#1
#2
#3
#4
#5
#6
#7
#8
Ratio of C-Caspase-3/ β-actin
0.80
0.75
0.70
0.65
0.60
0.55
0.38 0.39 0.40 0.41 0.42 0.43
Ratio of mature IL-16/ β-actin

Fig.5

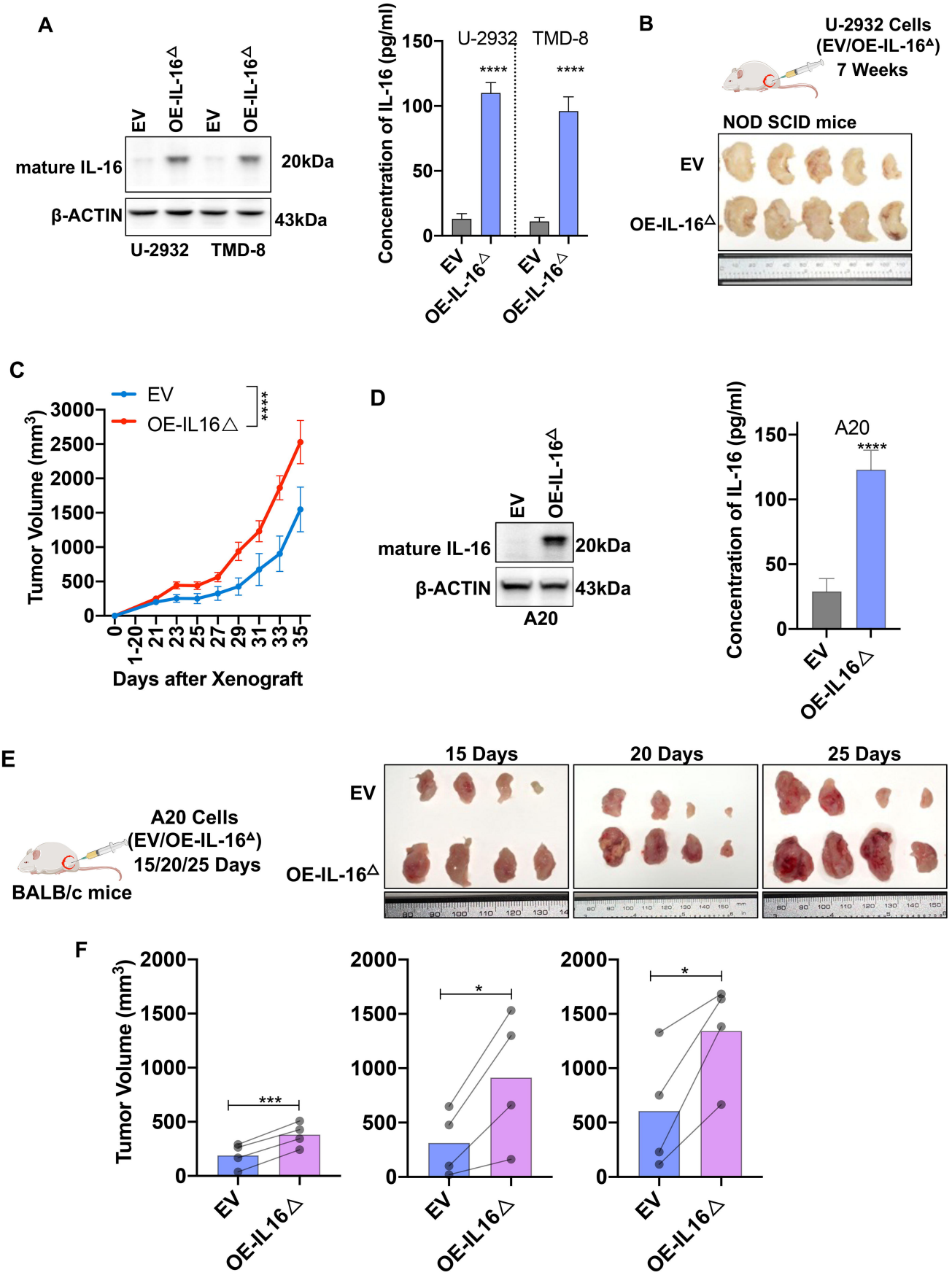
A
EV
OE-IL-16△
EV
OE-IL-16△
mature IL-16
20kDa
β-ACTIN
43kDa
U-2932
TMD-8
Concentration of IL-16 (pg/ml)
U-2932
TMD-8
****
****
EV
OE-IL-16△
EV
OE-IL-16△
B
U-2932 Cells
(EV/OE-IL-16△)
7 Weeks
NOD SCID mice
EV
OE-IL-16△
C
EV
OE-IL16△
****
Tumor Volume (mm3)
Days after Xenograft
D
EV
OE-IL-16△
mature IL-16
20kDa
β-ACTIN
43kDa
A20
Concentration of IL-16 (pg/ml)
A20
****
EV
OE-IL16△
E
A20 Cells
(EV/OE-IL-16△)
15/20/25 Days
BALB/c mice
15 Days
20 Days
25 Days
EV
OE-IL-16△
F
Tumor Volume (mm3)
***
*
*
EV
OE-IL16△
EV
OE-IL16△
EV
OE-IL16△

Fig.6

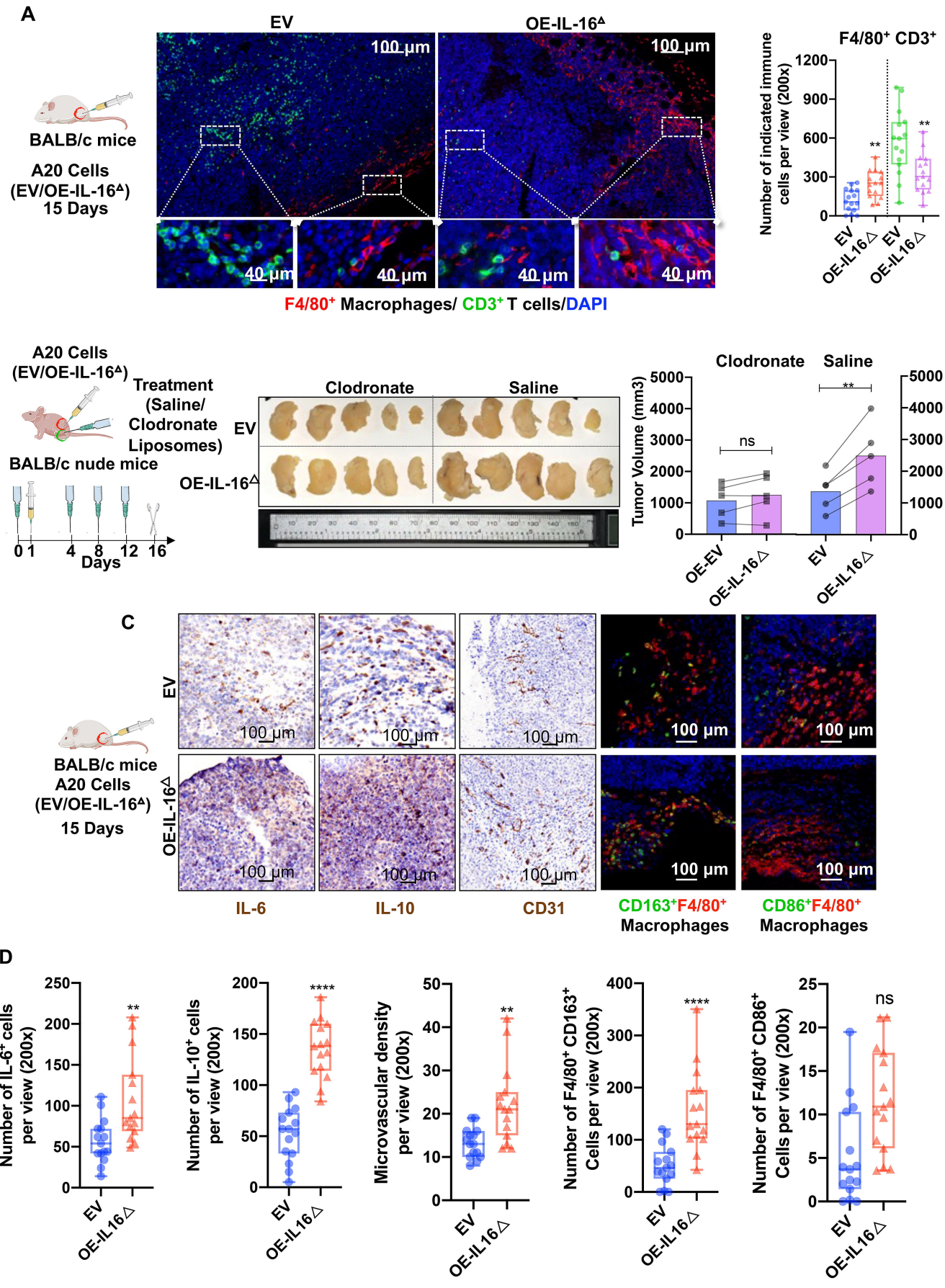
A
EV
OE-IL-16Δ
100 μm
40 μm
BALB/c mice
A20 Cells
(EV/OE-IL-16Δ)
15 Days
F4/80+ Macrophages/ CD3+ T cells/DAPI
F4/80+ CD3+
Number of indicated immune cells per view (200x)
EV
OE-IL16Δ
B
A20 Cells
(EV/OE-IL-16Δ)
Treatment
(Saline/
Clodronate
Liposomes)
BALB/c nude mice
0 1 4 8 12 16
Days
Clodronate
Saline
EV
OE-IL-16Δ
Tumor Volume (mm3)
ns
**
OE-EV
OE-IL-16Δ
C
BALB/c mice
A20 Cells
(EV/OE-IL-16Δ)
15 Days
IL-6
IL-10
CD31
CD163+F4/80+
Macrophages
CD86+F4/80+
Macrophages
D
Number of IL-6+ cells per view (200x)
Number of IL-10+ cells per view (200x)
Microvascular density per view (200x)
Number of F4/80+ CD163+ Cells per view (200x)
Number of F4/80+ CD86+ Cells per view (200x)
****
ns

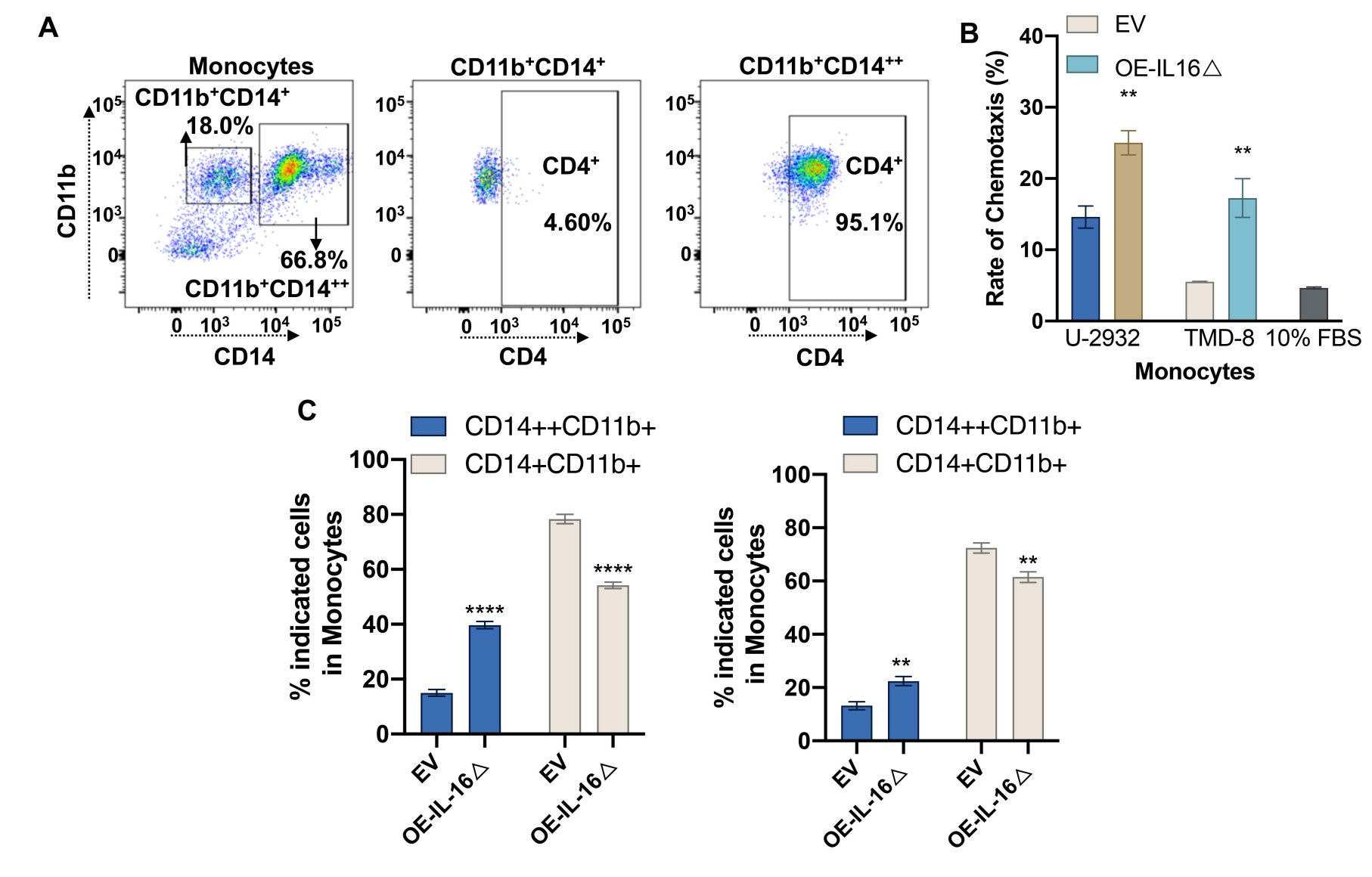
A
Monocytes
CD11b+CD14+
18.0%
66.8%
CD11b+CD14++
CD11b
CD14
CD11b+CD14+
CD4+
4.60%
CD4
CD11b+CD14++
CD4+
95.1%
CD4
B
EV
OE-IL16△
Rate of Chemotaxis (%)
U-2932
TMD-8
10% FBS
Monocytes
C
CD14++CD11b+
CD14+CD11b+
% indicated cells in Monocytes
EV
OE-IL-16△
CD14++CD11b+
CD14+CD11b+
% indicated cells in Monocytes
EV
OE-IL-16△

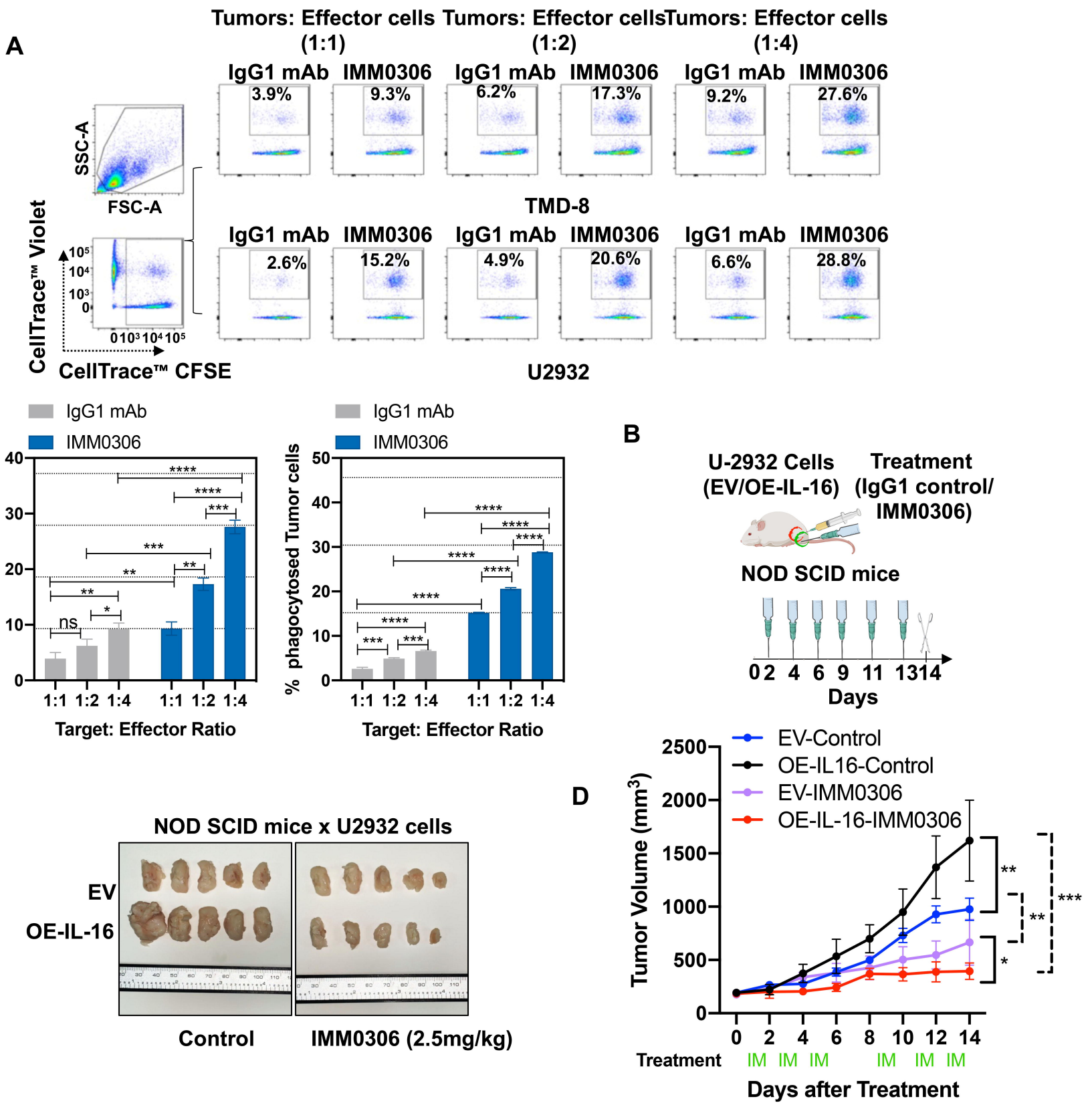
A
Tumors: Effector cells (1:1)
Tumors: Effector cells (1:2)
Tumors: Effector cells (1:4)
IgG1 mAb
IMM0306
3.9%
9.3%
6.2%
17.3%
9.2%
27.6%
SSC-A
FSC-A
CellTrace™ Violet
CellTrace™ CFSE
TMD-8
2.6%
15.2%
4.9%
20.6%
6.6%
28.8%
U2932
% phagocytosed Tumor cells
Target: Effector Ratio
1:1
1:2
1:4
B
U-2932 Cells (EV/OE-IL-16)
Treatment (IgG1 control/ IMM0306)
NOD SCID mice
0 2 4 6 9 11 13 14
Days
C
NOD SCID mice x U2932 cells
EV
OE-IL-16
Control
IMM0306 (2.5mg/kg)
D
EV-Control
OE-IL16-Control
EV-IMM0306
OE-IL-16-IMM0306
Tumor Volume (mm3)
Treatment
IM
Days after Treatment

Supplementray methods

Mice Models

For human DLBCL cells, the NOD SCID mice were inoculated subcutaneously on the right side with a mixture containing 5×10^6 tumor cells and Matrigel (354248, BD Biosciences, San Diego, CA, USA) (1:1). For murine DLBCL cells, the BALB/c nude mice or BALB/c mice were inoculated subcutaneously on the right side with 1×10^6 tumor cells in 200 μL PBS. When the tumors became palpable, tumor volumes (tumor volume = (length x width^2)/2) and body weight were measured at an interval of 1–2 days. Further, when the tumor volume reached a particular size, based on the ethical guidelines (The maximum diameter <20 mm), the mice were anesthetized and sacrificed, and the tumor samples were collected for further analysis.

For Clodronate Liposomes (a chemical depletion of macrophages in an animal model treatment, Yeasen, China, Cat#: 40337ES10)[1], the BALB/c nude mice were randomized (completely randomized by random number table) into two groups (5 mice/group): Clodronate Liposomes or Control treatment. For detail, mice were treated with 200μL Clodronate Liposomes (5mg/ml, i.p.) or saline (i.p.) treatment on Day0, and then the mice were inoculated subcutaneously on the right side with 1×10^6 A20 cells in 200 μL PBS on Day1. Furthermore, the mice were treated on Day4, 8 and Day12, and the mice were then anesthetized and sacrificed on Day16..

For IMM0306 (a fusion protein of CD20 mAb with the CD47 binding domain of SIRPα (V2) extracellular segment domain 1 (D1) on both heavy chains) treatment[2], when the tumors reached a mean of 200 mm^3, the NOD SCID mice which bear tumors were randomized (completely randomized by random number table) into Two groups (5 mice/group): Control and IMM0306. For detail, mice were treated with Control (human IgG1 control, 2.5mg/kg, i.v. Day2, 4, 6, 9, 11 and 13), IMM0306 (2.5mg/kg, i.v., Day2, 4, 6, 9, 11 and 13) respectively.

Cell lines culture

Human DLBCL cell lines, OCI-Ly3, U2932, TMD-8, Su-DHL6, Su-DHL10, and DoHH2 were kindly provided by Prof. Feng-Ting Liu (Tianjin Medical University Cancer Institute and Hospital, Tianjin, China), while murine DLBCL cell line A20, myeloma cell line RPMI-8226, human macrophage/monocyte cell line THP-1 cells, and 293T cell line were purchased from ATCC (Manassas, VA, USA). All the tumor cell lines and THP-1 cells were cultured in RPMI 1640 supplemented with 10–20% fetal bovine serum and 1% pen/strep at 37 °C in a humidified incubator with 5% CO_2, while the 293T cell line was cultured in DMEM supplemented with 10% fetal bovine serum and 1% pen/strep at 37 °C in a humidified incubator at 5% CO_2. Before culture, all the cell lines were validated via short tandem repeat analysis and tested for mycoplasma contamination.

Public databases and bioinformatics

We collected gene expression data of 1663 DLBCL patients (693 ABC-DLBCL and 970 GCB-DLBCL) from 4 GEO databases (GSE10846 [3], GSE31312 [4], GSE87371[5], and GSE117556 [6]), and empirical Bayes [7] was used to adjust batch effect, inSilicoMerging[8] was used to merge the databases, Limma was used to screen DEGs[9], R package clusterProfiler[10] was used to enrichment analysis of DEGs in KEGG pathway. R (version 4.0.5) was used for statistical computing and graphics.

Plasmid construction, virus production, and transduction

To construct IL-16 knockdown lentiviral vectors, the pLKO.1-Puro plasmid (8453, Addgene, Cambridge, MA, USA) was used. The shRNA-targeting human IL-16 (NM_004513.6) were 5'-GCCAGCCTGGTTTCGCCAAAG-3' for shRNA-#1; 5'-GGAGGAAGGTGCTGGTCTTGG-3' for shRNA-#2; 5'-GGGCCTCACACGGTTTGAAGC-3' for shRNA-#3; and 5'-TTCTCCGAACGTGTCACGT-3' for scrambled RNA.

Further, the pLVX-Puro plasmid (632164, ClonTech, Palo Alto, CA, USA) was used to construct the overexpression lentiviral vectors, human full-length IL-16 (NM_004513.6), human mature IL-16 (truncated human IL-16$^{\Delta 511\text{-}631aa}$ (NM_004513.6)), and murine mature IL-16 (truncated murine IL-16$^{\Delta 507\text{-}624aa}$ (NM_001360089.1)).

To produce lentiviruses in 293T cells, lentiviral vectors with the HIV packaging mix were transfected according to the manufacturer's protocol (LT001, GeneCopoeia Inc., Rockville, MD, USA). Supernatant samples were then harvested after 48 h following centrifugation

at 1,500 g, and incubated with the Lenti-X concentrator (631231, CloneTech, Palo Alto, CA, USA). Thereafter, lentiviruses were concentrated according to the manufacturer's instructions, aliquoted and frozen. The target cells were then transduced for 24 h by the lentiviruses using 5–10 μg/ml polybrene, after which the medium was replaced with a fresh complete medium. Then to select stably transduced cells, at 3–4 days intervals, the old medium was replaced with the fresh complete medium containing 1 μg/ml puromycin until drug-resistant colonies were obtained.

Immunohistochemistry (IHC), Immunohistochemical fluorescence (IHF) and multi-immunofluorescence staining(mIHC)

Tissue samples derived from the mouse model were formalin-fixed, paraffin-embedded, and sectioned (4-μm thickness). The tissue slides or tissue microarrays were de-paraffinized in xylene and rehydrated using graded ethanol followed by water before staining. Sections were then treated with a buffer as indicated for antigen retrieval in accordance with the instructions corresponding to the primary antibodies and with 3% H_2O_2 for the inactivation of endogenous peroxidase.

To perform IHC, after blocking for 30 min, sections were incubated with primary antibodies overnight at 4 °C. After washing, the sections were stained with a secondary antibody for 30 min at room temperature. Specifically, diaminobenzidine was used as a chromogen substrate, while hematoxylin was used for nuclear counterstaining. Finally, the sections were mounted with nail oil and viewed via microscopy.

Further, to realize IHF, after blocking for 30 min, tissue sections were incubated with primary antibodies overnight at 4 °C, and after washing, they were stained with a secondary antibody for 30 min at room temperature. Thereafter, they were rewashed and stained with the fluorophore-conjugated tyramide signal amplification reagent (G1226, Servicebio, Wuhan, China) for 10 min at room temperature. Then to perform multiple staining, a microwave oven was used to unmask the slices using 10 mM sodium citrate buffer (pH = 6.0) for 10 min, which thereafter, were incubated using another primary antibody, and the above procedure was repeated. Additionally, when it was necessary to realize multiplex plate staining or when only a single test was necessary, the sections were mounted in ProLong Gold anti-fade reagent with DAPI (P36941, Invitrogen, Carlsbad, CA, USA), and viewed via fluorescent microscopy.

The expression intensity and spatial distribution of CD20, CD3, CD68, IL-16 in tumor tissues and lymph node were labeled using mIHC with the Opal 7-color Manual IHC Kit (NEL801001KT, PerkinElmer) and VECTASHIELD® HardSet Antifade Mounting Medium (H-1400, Vector Labs) according to the manufacturer's protocol. Briefly, after the incubating with indicated primary antibodies and secondary antibody as IHC, the tissue sections were stained with Opal 7-coler Manual IHC Kit and remove the antibodies through microwaves. Repeat the above steps for another antibody, and mounted as IHF. The Fully automated quantitative pathology imaging system (Vectra Polaris, PerkinElmer) was used

to collected the data and TissueFAXS viewer (TissueGnostics GmbH) was used to analyse data.

RNA extraction, RT-PCR, and q-RT-PCR

RNA was extracted from the cells using Trizol reagent (15596018, Invitrogen, Carlsbad, CA, USA). The RNA pellets thus obtained were then resuspended in 20 μl of DNase- and RNase-free water, and Reverse Transcriptase-Polymerase Chain Reaction (RT-PCR) (RR036Q, Takara, Tokyo, Japan) as well as Real-time RT-PCR (q-RT-PCR) (RR430S, Takara, Tokyo, Japan) were performed on the extracted RNA according to the manufacturer's instructions. The primer sequences for IL-16 were 5'-GACACAGGGTTCTCGCTCAA-3' (forward) and 5'-GTCTTCCTTGGCTTCCGTGA-3' (reverse), while those for β-actin were 5'-ACACCTTCTACAATGAGCTG- 3' (forward) and 5'-CATGATGGAGTTGAAGGTAG-3' (reverse).

RNA-seq analysis

RNA samples (three biological replicates) were collected from U-2932 and TMD-8 cell lines with or without Pre-IL-16 knock-down. Thereafter, total RNA was extracted and used for RNA-seq analysis. The cDNA library was constructed and sequenced by Beijing Genomics Institute (BGI, Beijing, China) using the BGISEQ-500 platform, and high-quality reads were aligned to the human reference genome, GRCh38, using Bowtie2. Further, the expression levels of the different genes were normalized to fragments per kilobase of exon model per million mapped reads using RNA-seq via Expectation-

Maximization. Significant differentially expressed genes (DEGs) with absolute log2 ratio values ≥ 1 and the combination of Q values ≤ 0.05 were then confirmed using BGI Bioinformatics Service. RNA-seq data are available at SRA under BioProject ID: PRJNA786965 (https://www.ncbi.nlm.nih.gov/sra/PRJNA786965).

Cell viability assay

Cell viability was determined using the Cell Counting Kit-8 (CCK-8) (HY-K0301, MCE, Shanghai, China). Specifically, 10 μl of the CCK-8 reagent was added to the cell culture medium in 96-well plates for 2h, after which absorbance was measured at 450 nm using a microplate reader.

Flow cytometry

To determine the cell surface expression of the indicated protein, cells were incubated with TruStain FcX™ PLUS or Human TruStain FcX™ antibody (156603, 422301, Biolegend, San Diego, CA, USA) to block Fc receptors for 5min on ice. Thereafter, cells were stained with indicated antibodies, or relevant isotype controls on ice for 15 min in the dark, after which the cells were washed using PBS supplemented with 2% FBS and subjected to flow cytometry.

Further, to determine the percentage of apoptotic cells, DLBCL cells were stained with 7-AAD and Annexin V (640930, Biolegend, San Diego, CA, USA) according to the manufacturer's protocol, and thereafter subjected to flow cytometry. Further, to determine

caspase-3 and caspase-7 activation, DLBCL cells were stained with SYTOX™ AADvanced™ and CellEvent™ caspase 3/7 green detection reagent according to the manufacturer's protocol (C10427 Invitrogen, Carlsbad, CA, USA) and analyzed via flow cytometry.

Western blotting

Protein samples were extracted from tumor cell lines and tissues using CelLytic™ M cell Lysis Reagent (C2978, Sigma-Aldrich, St. Louis, MO, USA) and Tissue Extraction Reagent I (FNN0071, Invitrogen, Carlsbad, CA, USA), which is provided alongside protease and phosphatase inhibitor cocktails (78446, Invitrogen, Carlsbad, CA, USA). The extracted protein samples were loaded onto 4–12% SurePAGE™ Bis-Tris 10x8 gels (M00654, GenScript, Piscataway, NJ, USA) and within 5–10 min, transferred onto a 0.45-μM PVDF membrane (IPVH00010, Millipore, Billerica, MA, USA) using the eBlot™ L1 wet protein transfer system (L00686C, GenScript, Piscataway, NJ, USA). Thereafter, the PVDF membrane was blocked using the blocking buffer (5% polyvinyl pyrrolidone PVP, 5% fetal calf serum, and 0.1% sodium azide in tris-buffered solution [TBS] containing 0.2% Tween-20 [TBST]) for 60 min and then incubated with primary antibodies overnight at 4 °C. Bound antibodies were then detected via incubation using horseradish peroxidase-conjugated secondary antibodies in TBST.

Cytokine array and enzyme-linked immunosorbent assay (ELISA)

Serum samples from a patient with ABC-DLBCL collected at indicated time points were used for cytokine array analyses with human inflammation antibody array (40 Targets) (ab134003, Abcam, Cambridge, MA, USA) according to the manufacturer's instruction.

To determine serum IL-16 levels, ELISA was performed using the human IL-16 ELISA Kit (EH259RBX10, Invitrogen, Carlsbad, CA, USA) and murine IL-16 ELISA Kit (SEA062, Cloud-Clone Corp., Wuhan, China) following the manufacturer's instruction. In brief, serum samples were collected from DLBCL patients or the culture medium of DLBCL cell lines at indicated time points and subsequently subjected to ELISA in accordance with the manufacturer's protocol. Absorbances at 450 nm were then measured using a microplate reader.

Tumor cells isolation from tumor tissues

Tumor tissues were excised and digested post-mortem using a cocktail of 1 mg/mL collagenase type II (A004174, Sangon, Shanghai, China) and 0.02 mg/mL DNAase (10104159001, Sigma-Aldrich, St. Louis, MO, USA). After digestion at 37^{o}C for 30 minutes under continuous rotation (1,000rpm). Red Blood Cell Lysis Solution (130-094-183, Miltenyi Biotec, Shanghai, China) was to remove erythrocytes. Cells were passed through a 70-mm filter twice and then analyzed.

Isolation of Human Peripheral Blood Leucocyte (PBLs) and Human Blood Monocytes

Whole Blood from healthy donors was collected in Venous Blood Collection Tubes containing EDTA and stored immediately at 4 °C after collection. Red Blood Cell Lysis Solution (130-094-183, Miltenyi Biotec, Shanghai, China) was added to the whole Blood and incubated for 10 minutes at room temperature, and then centrifuge at 300xg for 10 minutes, and aspirate supernatant completely. Resuspend the cell pellet (PBLs) in PBS with 2% FBS and passed through a 70-mm filter twice for further analysis.

Monocytes were isolated by Dynabeads® Untouched™ Human Monocytes kit (11350D, Invitrogen, Carlsbad, CA, USA) according to the manufacturer's protocol. Briefly, $5x10^7$ PBLs were mixed with blocking reagent and antibody mix, and incubated for 20min at 4 °C. Wash the cells and mixed them with pre-washed Dynabeads, and incubate them for 15min at 4 °C. Resuspend the bead-bound cells thoroughly and placed the tube in the magnet for 2min. Transfer the supernatant containing the untouched human monocytes, to a new larger tube. Monocytes were used for further analysis.

Antibody-dependent cellular phagocytosis (ADCP)

Effector cells (THP-1 cells, a human macrophage/monocyte cell line) and DLBCL cells were labeled with CellTrace™ Violet and CellTrace™ CFSE (C34554, C34557, Invitrogen, Carlsbad, CA, USA) respectively according to the manufacturer's protocol. Aliquot labeled DLBCL cells and effector cells at the indicated ratio in a 96-well round-bottom plate, and add the IMM0306 (ImmuneOnco, Shanghai, China) or IgG1 mAb (BE0297, Bio X Cell, Lebanon, NH, USA) in the plate. Incubate the plate for 30min at 37°C in a 5% CO2

incubator. Wash the cells with PBS supplemented with 2% FBS and proceed to analysis on a flow cytometer. The double-stained cells were phagocytosed tumor cells.

In Vitro Cell Migration Assay

Cells were washed in PBS, centrifuged at 300xg for 5 minutes, and resuspended in 0.1% BSA RPMI-1640 medium. Transwell chambers (5μm core, 3421, Corning, NY, USA) were prepared to fill with 500 μL of indicated CM in the lower chamber. 100 μL $5x10^5$ cells were plated in the upper insert of each Transwell chamber and incubated at 37°C for 1h. Relative cell numbers of the lower chamber were determined using the Cell Counting Kit-8 (CCK-8) (HY-K0301, MCE, Shanghai, China) and the absorbance was measured at 450 nm using a microplate reader. Rate of chemotaxis (%)=($OD_{Lower\ chamber}$-$OD_{Background}$/ $OD_{Upper\ chamber}$-$OD_{Background}$)x100.

Statistical analysis

Data were presented as either mean or median ± SEM or SD, and statistical significance was determined by performing the two-tailed Student's paired or unpaired t-test, one-way or two-way ANOVA, and the Chi-square test. Further, Pearson product-moment correlation analysis was employed to analyze the linearity of the correlation between the two groups. To perform categorical analysis, i.e., divide patients into two cohorts based on serum IL-16 levels, the X-tile statistical package was used[11]. Outcomes, which were measured from the date of diagnosis to the date of adverse event occurrence or last follow-up, included overall survival (OS) and patient free survival (PFS) rates, and Log-rank

(Mantel-Cox) test and Cox regression were used to evaluate the relationship between the clinical features or gene expressions and OS or PFS. Sample sizes were determined according to pilot studies and based on previous experimental experiences. Experiments were biologically replicated three times in the cell-level study. For *in vitro* studies, the sample size in each group was at least 3, for *in vivo* studies, the sample size in each group was at least 4, and for the studies of tumor therapeutic outcomes, the sample size in each group was at least 5. For all the different statistical analyses, $P < 0.05$ were considered significant, $^{*}P < 0.05$, $^{**}P < 0.01$; $^{***}P < 0.001$, and $^{****}P < 0.0001$. Data analyses were performed using Prism software (Version of 9, GRAPH PAD Software Inc., San Diego, CA, USA) and SPSS software (Version of 24, IBM, Armonk, NY, USA).

References

1. Moreno SG. Depleting Macrophages In Vivo with Clodronate-Liposomes. *Methods Mol Biol*. 2018;1784:259-262.
2. Yu J, Li S, Chen D, et al. IMM0306, a fusion protein of CD20 mAb with the CD47 binding domain of SIRPalpha, exerts excellent cancer killing efficacy by activating both macrophages and NK cells via blockade of CD47-SIRPalpha interaction and FcγR engagement by simultaneously binding to CD47 and CD20 of B cells. *Leukemia*. 2023;37(3):695-698.
3. Lenz G, Wright G, Dave SS, et al. Stromal gene signatures in large-B-cell lymphomas. *N Engl J Med*. 2008;359(22):2313-2323.
4. Xu-Monette ZY, Moller MB, Tzankov A, et al. MDM2 phenotypic and genotypic profiling, respective to TP53 genetic status, in diffuse large B-cell lymphoma patients treated with rituximab-CHOP immunochemotherapy: a report from the International DLBCL Rituximab-CHOP Consortium Program. *Blood*. 2013;122(15):2630-2640.
5. Dubois S, Viailly PJ, Bohers E, et al. Biological and Clinical Relevance of Associated Genomic Alterations in MYD88 L265P and non-L265P-Mutated Diffuse Large B-Cell Lymphoma: Analysis of 361 Cases. *Clin Cancer Res*. 2017;23(9):2232-2244.

6. Sha C, Barrans S, Cucco F, et al. Molecular High-Grade B-Cell Lymphoma: Defining a Poor-Risk Group That Requires Different Approaches to Therapy. *J Clin Oncol*. 2019;37(3):202-212.
7. Johnson WE, Li C, Rabinovic A. Adjusting batch effects in microarray expression data using empirical Bayes methods. *Biostatistics*. 2007;8(1):118-127.
8. Taminau J, Meganck S, Lazar C, et al. Unlocking the potential of publicly available microarray data using inSilicoDb and inSilicoMerging R/Bioconductor packages. *BMC Bioinformatics*. 2012;13:335.
9. Ritchie ME, Phipson B, Wu D, et al. limma powers differential expression analyses for RNA-sequencing and microarray studies. *Nucleic Acids Res*. 2015;43(7):e47.
10. Yu G, Wang LG, Han Y, He QY. clusterProfiler: an R package for comparing biological themes among gene clusters. *OMICS*. 2012;16(5):284-287.
11. Camp RL, Dolled-Filhart M, Rimm DL. X-tile: a new bio-informatics tool for biomarker assessment and outcome-based cut-point optimization. *Clin Cancer Res*. 2004;10(21):7252-7259.

Supplementray tables

Supplementray Table 1. Key reagent or resources

Reagent or Resource	Source	Identifier
Antibodies and recombinant protein		
Rabbit monoclonal anti-IL-16 [EPR19988]	Abcam	Cat#: ab207181
Mouse IL-16 Biotinylated Antibody	R&D	Cat#: BAF1727
Caspase-3 Antibody	CST	Cat#: 9662
Cleaved Caspase-3 (Asp175) (5A1E) Rabbit mAb	CST	Cat#: 9661
β-Actin (8H10D10) Mouse mAb	CST	Cat#: 3700
Anti-rabbit IgG, HRP-linked Antibody	CST	Cat#: 7074
Anti-mouse IgG, HRP-linked Antibody	CST	Cat#: 7076
F4/80 (D2S9R) XP® Rabbit mAb	CST	Cat#: 70076
CD3ε (E4T1B) XP® Rabbit mAb	CST	Cat#: 78588
CD3ε (D7A6E™) XP® Rabbit mAb	CST	Cat#: 85061
CD4 (D7D2Z) Rabbit mAb	CST	Cat#: 25229
CD8α (D4W2Z) XP® Rabbit mAb	CST	Cat#: 98941
CD11c (D1V9Y) Rabbit mAb	CST	Cat#: 3850
Anti-MS4A1 antibody produced in rabbit	Sigma	Cat#: HPA014341
CD68 (E3O7V) Rabbit mAb	CST	Cat#: 97778
FoxP3 (D6O8R) Rabbit mAb	CST	Cat#: 12653
Granzyme B (E5V2L) Rabbit mAb	CST	Cat#: 3850
Ly-6G (E6Z1T) Rabbit mAb	CST	Cat#: 87048
T-bet/TBX21 (E4I2K) Rabbit mAb	CST	Cat#: 97135

Siglec-H Antibody (23M15C8)	R&D	Cat#: NBP2-27062
CD31 (PECAM-1) (D8V9E) XP® Rabbit mAb	CST	Cat#: 77699
CD86 (E5W6H) Rabbit mAb	CST	Cat#: 19589
Anti-CD163 antibody [EPR19518]	Abcam	Cat#: ab182422
Anti-IL-6 antibody [1.2-2B11-2G10]	Abcam	Cat#: ab9324
Anti-IL-10 antibody [JES5-2A5]	Abcam	Cat#: ab189392
Goat anti-Rabbit IgG (H+L) Secondary Antibody, HRP	invitrogen	Cat#: 31460
Goat anti-Mouse IgG (H+L) Secondary Antibody, HRP	invitrogen	Cat#: 31430
Pacific Blue™ anti-human CD8 Antibody	Biolegend	Cat#: 344717
FITC Mouse Anti-Human CD4	BD	Cat#: 555346
APC anti-human CD14 Antibody	Biolegend	Cat#: 325607
PE/Cyanine7 anti-human CD3	Biolegend	Cat#: 980010
PE anti-human CD9 Antibody	Biolegend	Cat#: 312105
PE anti-human CD4 Antibody	Biolegend	Cat#: 300508
PE anti-human CD138 (Syndecan-1) Antibody	Biolegend	Cat#: 352305
PE anti-human CD19 Antibody	Biolegend	Cat#: 302254
APC/Cyanine7 anti-human CD11b Antibody	Biolegend	Cat#: 301341
Human TruStain FcX™ (Fc Receptor Blocking Solution)	Biolegend	Cat#: 422301
Recombinant human IL-16 protein (Active) (ab256039)	Abcam	Cat#: ab259416
InVivoMAb human IgG1 isotype control	Bio X Cell	Cat#: BE0297
Chemicals		

Vincristine sulfate	MCE	Cat#: HY-N0488
Doxorubicin hydrochloride	MCE	Cat#: HY-15142
4-Hydroperoxy Cyclophosphamide	Santa Cruz	Cat#: 39800-16-3
PAC-1	MCE	Cat#: HY-13523
Matrigel matrix high protein	BD	Cat#: 354248
Streptavidin (HRP)	Abcam	Cat#: ab7403
Puromycin Dihydrochloride	MCE	Cat#: HY-B1743A
Polybrene	Santa Cruz	Cat#: sc-134220
Clodronate Liposomes	Yeasen	Cat#: 40337ES10
APC Annexin V	Biolegend	Cat#: 640941
7-AAD	BD	Cat#: 559925
DAPI Solution	BD	Cat#: 564907
Critical commerical assays		
Lenti-Pac HIV Expression Packaging Kit	GeneCopoeia	Cat#: LT001
TSA Plus muti-flurophore detectiong kit	Servicebio	Cat#: G1226
Human IL-16 ELISA Kit	invitrogen	Cat#: EH259RB
ELISA Kit for Interleukin 16 (IL16)	Cloud-Clone Corp.	Cat#: SEA062Mu
CellEvent™ Caspase 3/7 Green Ready Flow™ Reagent	invitrogen	Cat#: R37167

Human Inflammation Antibody Array (40 Targets)	Abcam	Cat#: ab134003
Dynabeads® UntouchedTM Human Monocytes kit	invitrogen	Cat#: 11350D
CellTrace™ CFSE Cell Proliferation Kit, for flow cytometry	invitrogen	Cat#: C34554
CellTrace™ Violet Cell Proliferation Kit	invitrogen	Cat#: C34557

Supplementray Table 2. Baseline clinical characteristics of *de novo* patients with ABC-DLBCL or GCB DLBCL

Characteristic	ABC-DLBCL (n=45)		GCB-DLBCL (n=39)	
	n	**(% of total)**	**n**	**(% of total)**
Age, y				
⩽60	23	51.11	27	69.23
>60	22	48.89	12	30.77
Sex				
Male	26	57.78	22	56.41
Female	19	42.22	17	43.59
ECOG PS				
⩽1	40	88.89	23	58.97
>1	5	11.11	16	41.03
Serum LDH level				
Normal	25	55.56	23	58.97
Elevated	20	44.44	16	41.03
Serum β2M level				

Normal	19	42.22	23	58.97
Elevated	19	42.22	9	23.08
Unknown	7	15.56	7	17.95
Ann Arbor stage				0.00
I/II	14	31.11	22	56.41
III/IV	31	68.89	17	43.59
B symptoms				
Absent	30	66.67	28	71.79
Present	15	33.33	11	28.21
IPI				
<2	19	42.22	22	56.41
⩾2	26	57.78	17	43.59
No. of identified extranodal sites				
<2	31	68.89	29	74.36
⩾2	14	31.11	10	25.64
DEL				
Absent	33	73.33	32	82.05
Present	12	26.67	7	17.95
Treatment				
R-CHOP	23	51.11	18	46.15
R-EDOCH	20	44.44	21	53.85
R-miniCHOP	2	4.44	0	0.00
Therapeutic response				
CR	33	73.33	35	89.74

PR	7	15.56	1	2.56
SD+PD	4	8.89	1	2.56
Unknown	1	2.22	2	5.13

ECOG PS, Eastern Cooperative Oncology Group performance status; IPI, International Prognostic Index; LDH, lactate dehydrogenase; DEL, double expression lymphoma (MYC and BCL2 protein expression).

Supplementray figures

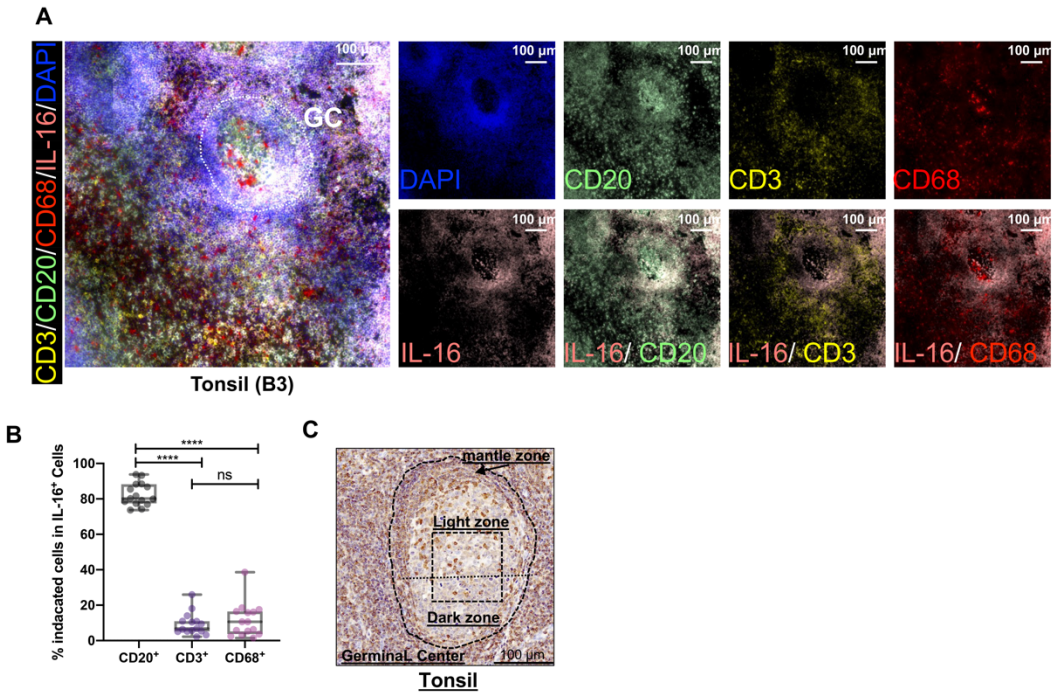

fig. S1. (A) Representative mIHC images for IL-16 protein expression (pink pseudocolor) in tonsil specimens. CD20 (B cells, green pseudocolor), CD3 (T cells, yellow pseudocolor), CD68 (macrophages, red pseudocolor), and DAPI nuclear stain (blue pseudocolor) included to discern tissue landscape. Scale bars apply across each row. (B) Proportion of IL-16-positive cells in different types of immune cells. n=15. (C) Representative IHC images for IL-16 protein expression in tonsil specimens. Data shown are mean ± SD. p values are based on unpaired t-test. ns=non-significant; *p < 0.05, **p < 0.01, ***p < 0.001, ****p < 0.0001.

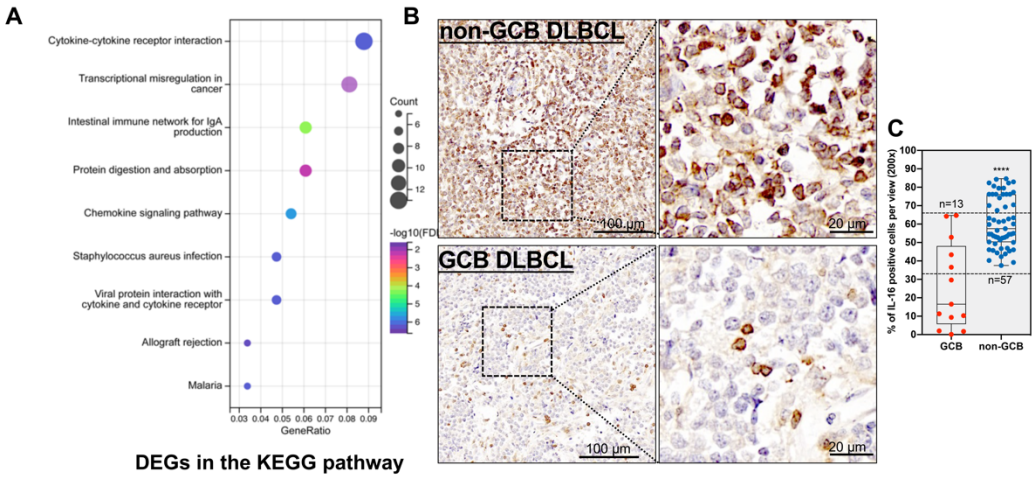

fig. S2. (A) The bubble diagram indicates the enrichment analysis of DEGs in KEGG pathway by clusterProfiler. （B-C）Representative IHC and quantification for IL-16 protein expression in DLBCL tissues. Boxed regions are magnified right. Scale bars apply across each row. The difference of IL-16 positive cells between GCB DLBCL (n=13) and non-GCB DLBCL (n=57) is analyzed. Data shown are mean ± SD. p values are based on unpaired t-test. ns=non-significant; *p < 0.05, **p < 0.01, ***p < 0.001, ****p < 0.0001.

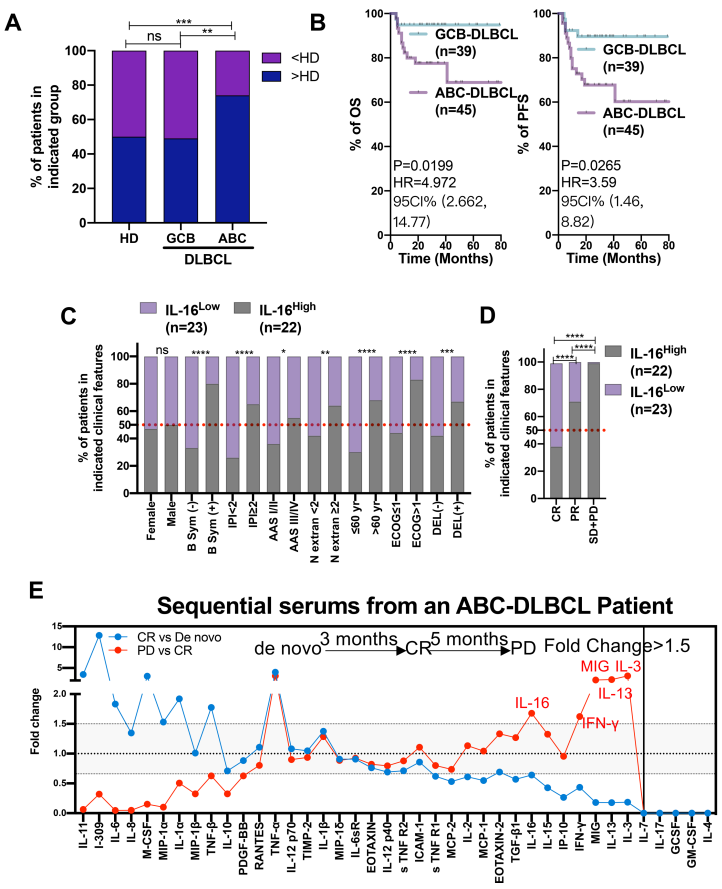

fig. S3. (A) Detection of the levels of IL-16 in serum from DLCBL patients (39 GCB-DLBCL and 45 ABC-DLBCL) and health donors (n=10) by ELISA. Proportion of patients in indicated group (the mean of IL-16 levels in the serum of healthy donors was used as a basis for grouping). (B) OS and PFS of DLBCL patients based COO. (C) The differences in serum IL-16 of ABC-DLBCL patients between indicated clinical features are analyzed. (D) The differences in serum IL-16 of ABC-DLBCL patients between the response to treatment are analyzed. (E) Determination of the relative differences (fold change) of 40 cytokines in sequential serums from an ABC-DLBCL patient between different time points (CR vs de novo and PD vs CR) by human inflammation antibody

array. Red symbols are cytokines that are markedly varied in the two comparisons (> 1.5 fold change). p values are based Pearson correlation, Chi-square test, and Cox regression. ns=non-significant; *p < 0.05, **p < 0.01, ***p < 0.001, ****p < 0.0001.

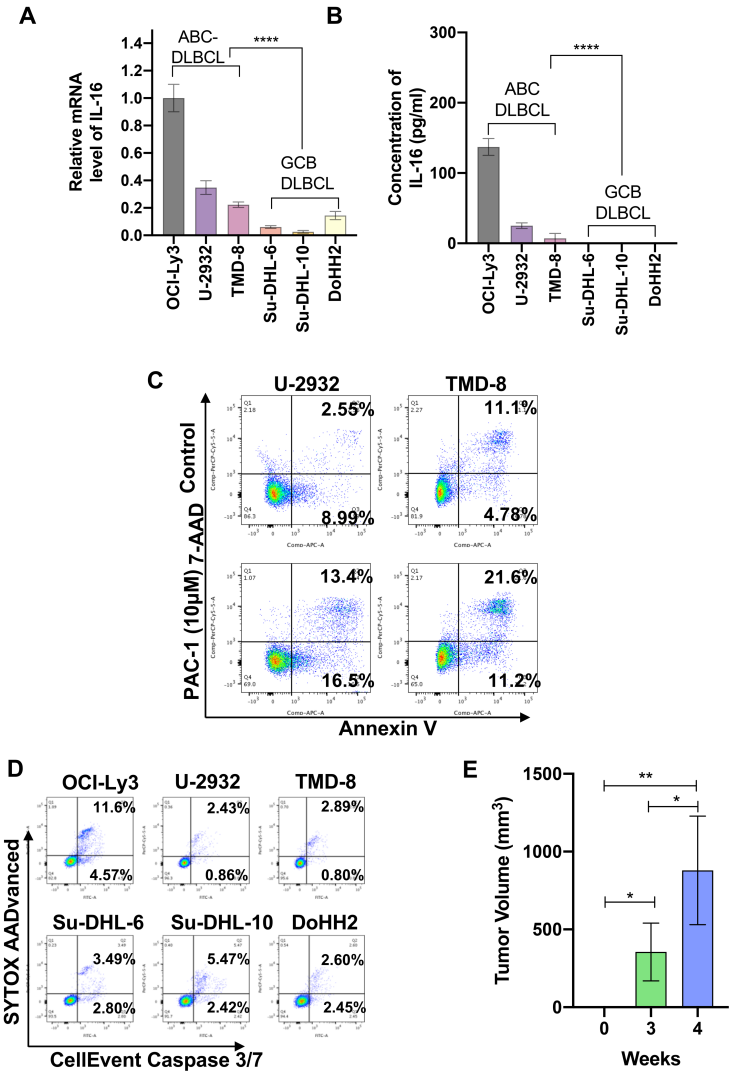

fig. S4. (A) Secretion levels of IL-16 in the culture medium of DLBCL cell lines (OCI-Ly3, TMD-8, U-2932, Su-DHL-6, Su-DHL-10, and DoHH2) ($5x10^5$ cells/ml, 24h) are quantified by ELISA. (B) IL-16 transcript levels in DLBCL cell lines (OCI-Ly3, TMD-8, U-2932, Su-DHL-6, Su-DHL-10, and DoHH2) are quantified by qPCR and normalized to

the expression in OCI-Ly3 cells. β-Actin serves as a reference gene. (C) ABC-DLBCL cell lines (U-2932 and TMD-8) are treated with 10μM PAC-1 or DMSO for 24 h, and percentages of apoptosis are determined by flow cytometry (Annexin V and 7-AAD double staining) and analyzed by Flowjo. (D) Caspase-3/7 activation of untreated DLBCL cell lines (OCI-Ly3, U-2932, TMD-8, Su-DHL-6, Su-DHL-10, and DoHH2) is determined by flow cytometry (CellEvent Caspase-3/7 and SYTOX AADvanced double staining) and analyzed by Flowjo. (E) The BALB/c mice were inoculated subcutaneously with A20 cells (n=4/group), the serum was collected at different time points (week0, week3 and week4), and the tumor tissues were collected at different time points (week3 and week4). Data shown are mean ± SD. p values are based on one-way ANOVA and unpaired t-test. ns=non-significant; *$p < 0.05$, **$p < 0.01$, ***$p < 0.001$, ****$p < 0.0001$.

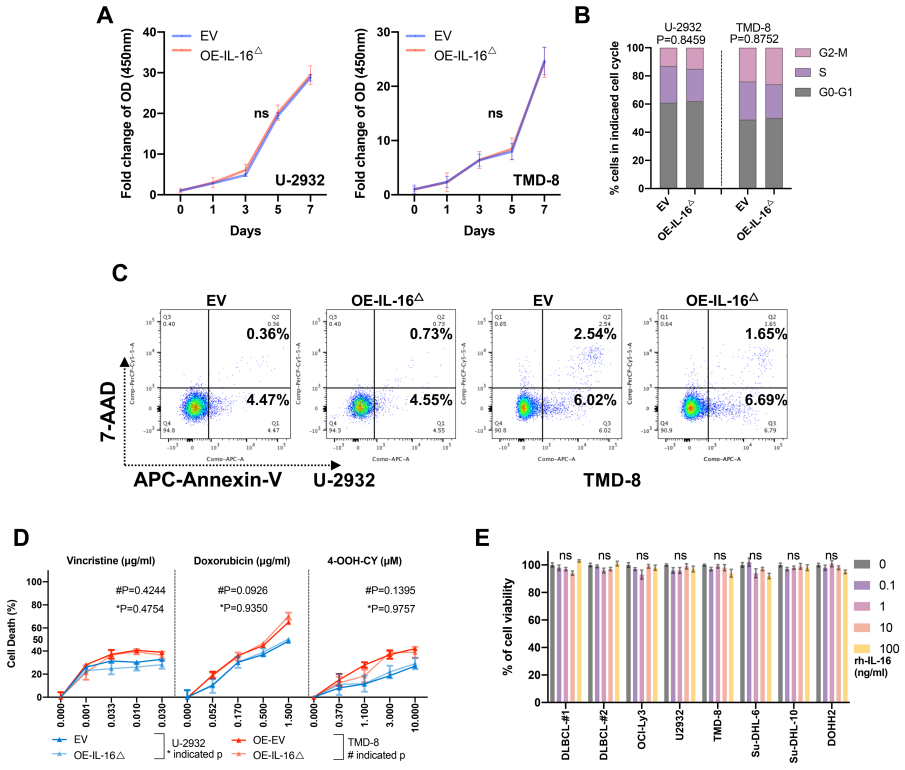

fig. S5. (A-D) U-2932 and TMD-8 with stable overexpression of IL-16$^{\triangle 511\text{-}631aa}$ (labeled with IL-16$^{\triangle}$) or EV are cultured *in vitro*. **(A)** OD of cells mixed with CCK-8 was determined at indicated time points. Fold change=($OD_{Day\text{-}n}$-$OD_{background}$)/ ($OD_{Day\text{-}0}$-$OD_{background}$)**. (B)** The cell cycle is determined by flow cytometry (DAPI staining) and analyzed by Flowjo. **(C)** Apoptosis is determined by flow cytometry (Annexin V-APC and 7-AAD double staining) and analyzed by Flowjo. **(D)** Cells are treated with indicated doses of Vincristine, Doxorubicin, 4-OOH-CY, or DMSO for 24 h, and percentages of cell death are determined by the CCK-8 test. **(E)** Primary cells from 2 DLBCL tissues and DLBCL cell lines (OCI-Ly3, TMD-8, U-2932, Su-DHL-6, Su-DHL-10, and DoHH2) are treated with indicated doses of rh-IL-16 for 24 h, and percentages of cell viability are

determined by the CCK-8 test. Data shown are mean ± SD. p values are based on the one-way or two-way ANOVA and Chi-square test.

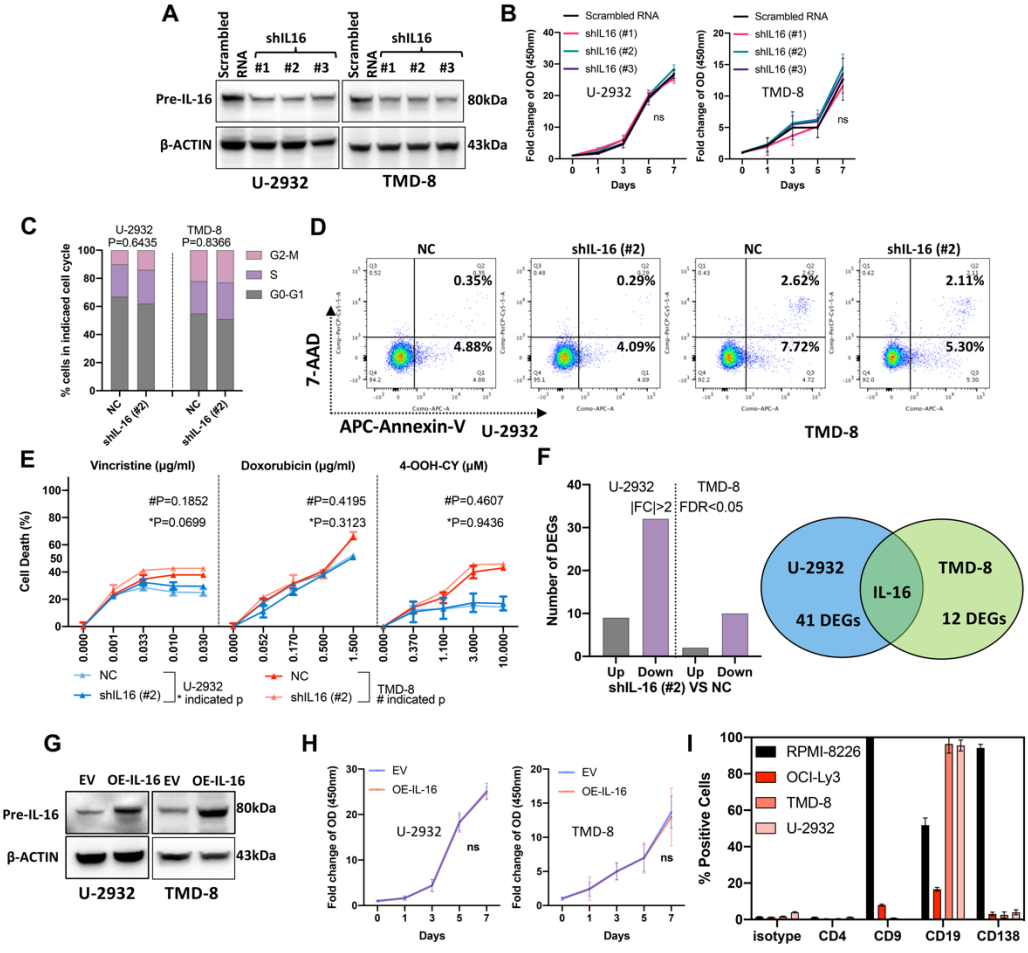

fig. S6. (A) Detection of IL-16 protein expression by western blotting in DLBCL cell lines (U-2932 and TMD-8) with stable Pre-IL-16 expression knockdown (shIL16 #1, #2 and #3) or NC. β-Actin is used as a loading control. NC (Negative Control) indicated scrambled RNA (B-F) U-2932 and TMD-8 cells with stable Pre-IL-16 expression knockdown or NC are cultured *in vitro*. (B) Optical density (OD) of cells mixed with CCK-8 were determined at indicated time points. Fold change=($OD_{Day\text{-}n}$-$OD_{background}$)/

(OD_{Day-0}-$OD_{background}$). (C) The cell cycle is determined by flow cytometry (DAPI staining) and analyzed by Flowjo. (D) Apoptosis is determined by flow cytometry (Annexin V-APC and 7-AAD double staining) and analyzed by Flowjo. (E) Cells are treated with indicated doses of Vincristine, Doxorubicin, 4-OOH-CY, or DMSO for 24 h, and percentages of cell death are determined by the CCK-8 test. (F) RNA-seq is used to detect differential expression genes (DEGs). Numbers of genes are upregulated (Up) or downregulated (Down) by Pre-IL-16 expression knockdown ($|FC| > 2$, $FDR < 0.05$). The Venn diagram was shown the overlap between DEGs detected in U-2932 cell lines and TMD-8 cell lines. (G) Detection of IL-16 protein expression by western blotting in DLBCL cell lines (U-2932 and TMD-8) with stable overexpression of Pre-IL-16 or NC. β-Actin is used as a loading control. NC indicated empty vector controls. (H) U-2932 and TMD-8 cells with stable Pre-IL-16 expression overexpression or NC are cultured *in vitro*. Optical density (OD) of cells mixed with CCK-8 were determined at indicated time points. Fold change=(OD_{Day-n}-$OD_{background}$)/ (OD_{Day-0}-$OD_{background}$). (I) Determination of CD4, CD9, CD19 and CD138 expression on three ABC-DLBCL cell lines (OCI-Ly3, TMD-8, and U-2932) and myeloma cells (RPMI-8226) by flow cytometry. Cells are stained with anti-CD4, CD9, CD19 and CD138 antibodies (PE) or mouse IgG-PE control isotype respectively. Data shown are mean ± SD. p values are based on the one-way or two-way ANOVA, Chi-square test, unpaired or paired t-test. ns=non-significant; *$p < 0.05$, **$p < 0.01$, ***$p < 0.001$, ****$p < 0.0001$.

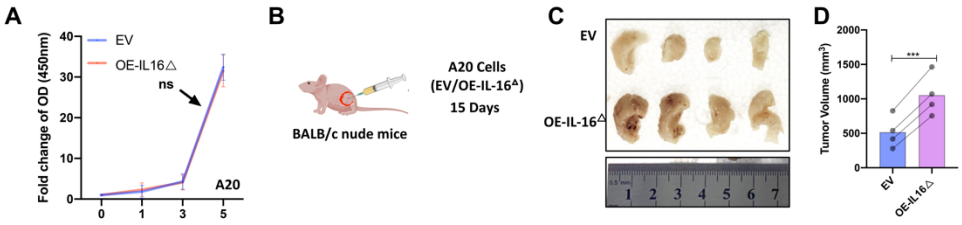

fig. S7. (A) A20 cells with stable overexpression of murine IL-16$^{\Delta 507\text{-}624aa}$ or EV are cultured *in vitro* and percentages of cell viability are determined by the CCK-8 test. (B-D) BALB/c nude mice are inoculated with A20 cells with murine IL-16$^{\Delta 507\text{-}624aa}$ overexpression or EV respectively for 15 days (n=4/group). A collection of tumors and tumor volumes from mice. Data shown are mean ± SD. p values are based on the one-way or two-way ANOVA and paired t-test. ns=non-significant; *$p < 0.05$, **$p < 0.01$, ***$p < 0.001$, ****$p < 0.0001$.

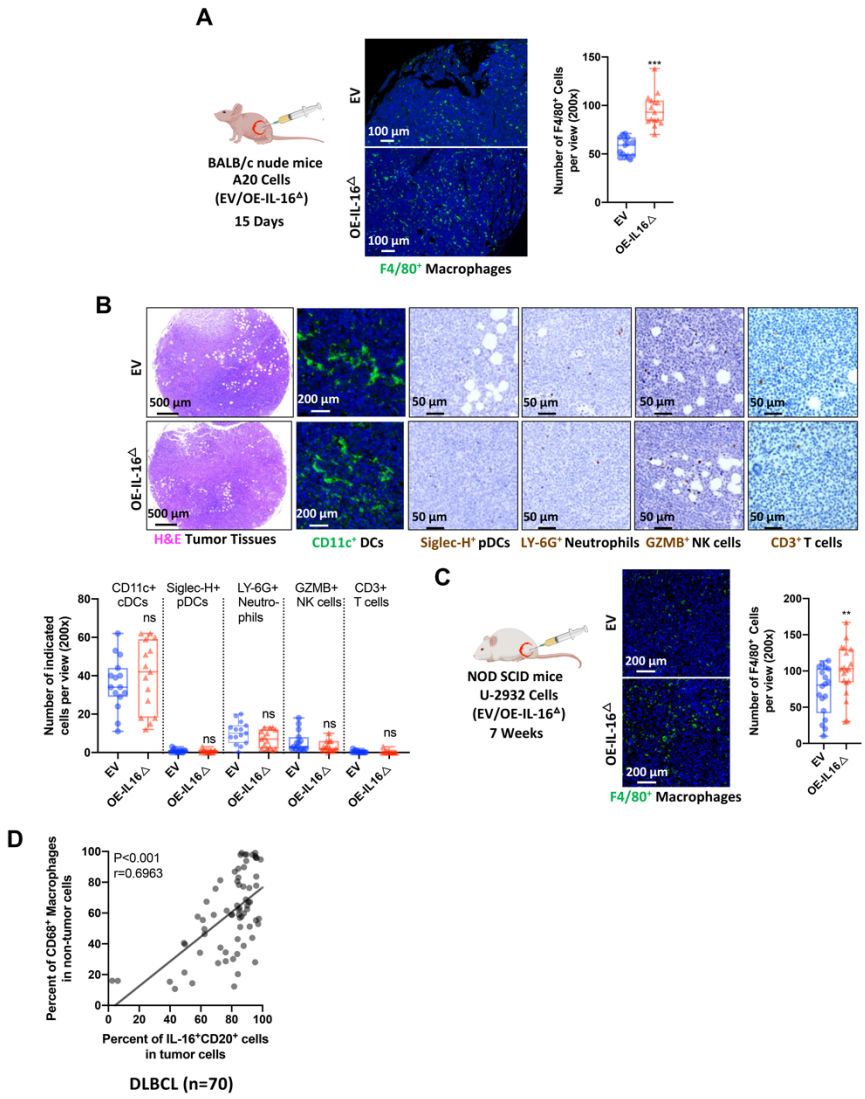

fig. S8. (A) Representative immunostaining and quantificationfor the F4/80^{+} macrophages in sections of tumor tissues from BALB/c nude mice. The differences in the infiltration of F4/80^{+} macrophages in indicated tumor tissues between different groups (murine IL-16$^{\Delta 507\text{-}624aa}$ overexpression vs EV) are analyzed. (B) Representative stain for H&E in the sections of indicated tumor tissues from BALB/c nude mice. Representative immunostaining and quantification for the indicated immune cells of tumor tissues from BALB/c nude mice. The differences in the infiltration of indicated immune cells in

indicated tumor tissues between different groups (murine IL-16$^{\Delta 507\text{-}624aa}$ overexpression vs EV) are analyzed. (C) Representative immunostaining and quantification for the F4/80^{+} macrophages in sections of tumor tissues from NOD SCID mice. The differences in the infiltration of F4/80^{+} macrophages in indicated tumor tissues between different groups (IL-16$^{\Delta 511\text{-}631aa}$ overexpression vs EV) are analyzed. (D) The correlation between the proportion of IL-16^{+}CD20^{+} cells in tumour cells and the proportion of CD68^{+} macrophages in non-tumour cells as shown in Figure 2D. (n=70). Data shown are mean ± SD. p values are based on unpaired t-test and Pearson correlation.. ns=non-significant; *p < 0.05, **p < 0.01, ***p < 0.001, ****p < 0.0001.

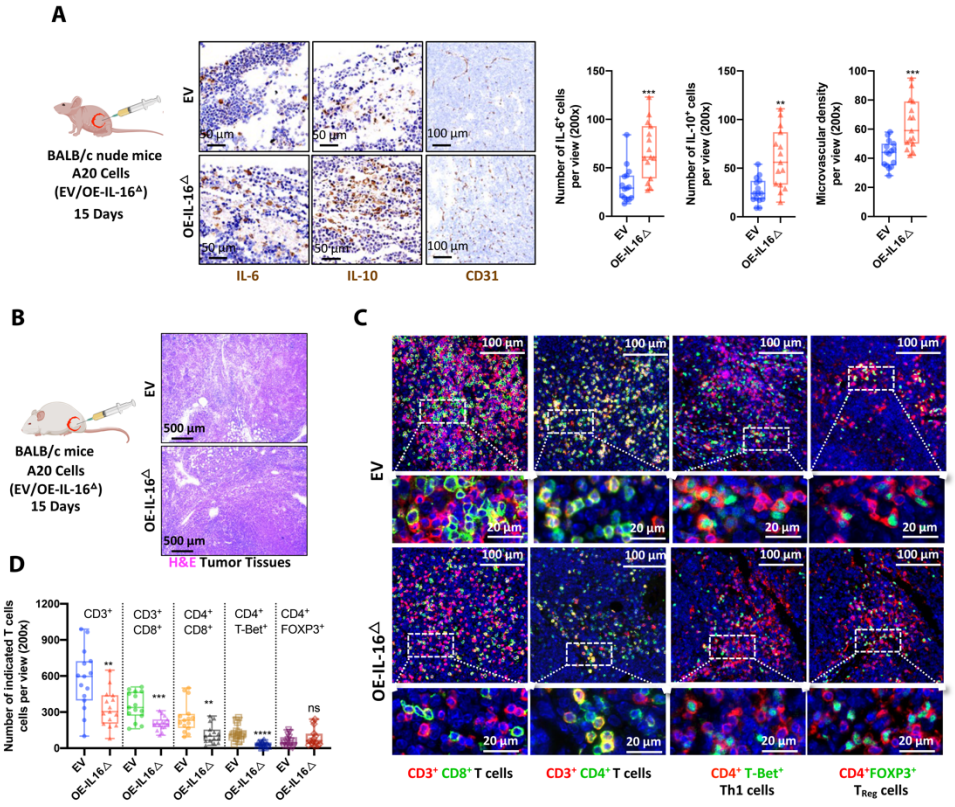

fig. S9. (A) Representative immunostaining and quantification for the cytokines IL-6 and IL-10, and vascular endothelial cells marker CD31 (microvascular density) in the sections of tumor tissues from BALB/c nude mice. The difference in the infiltration of indicated cells in tumor tissues between different groups (murine IL-16$^{\Delta 507\text{-}624aa}$ overexpression vs EV) is analyzed. (B) Representative stain for H&E in the sections of indicated tumor tissues from BALB/c mice. (C-D) Representative immunostaining and quantification for CD3 and CD8, CD3 and CD4, CD4 and T-Bet, and CD4 and FOXP3 in the sections of tumor tissues. The difference in the infiltration of indicated cells in tumor tissues between different groups (murine IL-16$^{\Delta 507\text{-}624aa}$ overexpression vs EV) is analyzed. Scale bars apply across each row.Data shown are mean ± SD. p values are based on unpaired t-test. ns=non-significant; *p < 0.05, **p < 0.01, ***p < 0.001, ****p < 0.0001.

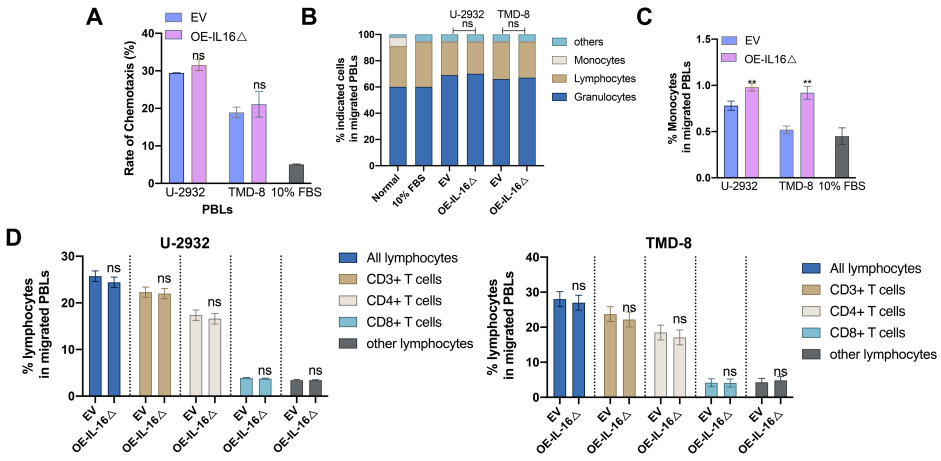

fig. S10. (A) The culture medium of indicated DLBCL cells (U-2932 and TMD-8 cells with stable overexpression of IL-16$^{\Delta 511\text{-}631aa}$ or EV, 5x10^5 cells/ml, 24h) was collected and used as chemokines. Cell migration of peripheral blood leucocyte (PBLs) is

determined by transwell assay (1h) combined with the CCK-8 test. 10% FBS culture medium were used as control. Rate of chemotaxis (%)=($OD_{Lower\ chamber}$-$OD_{Background}$/ $OD_{Upper\ chamber}$-$OD_{Background}$)x100. (B-D) Migrated PBL is stained with anti-CD3-PE-Cy7, anti-CD4-FITC, anti-CD8-Pacific blue, anti-CD11b-APC-Cy7, and anti-CD14-APC antibodies and analyzed by Flow cytometry to distinguish monocytes, lymphocytes, and granulocytes. (B) the proportion of monocytes, lymphocytes, and granulocytes in migrated PBLs. (C) the proportion of monocytes in migrated PBLs. (D) the proportion of indicated T cells in migrated PBLs. Data shown are mean ± SD. p values are based on unpaired t-test and Chi-square test. ns=non-significant; *p < 0.05, **p < 0.01, ***p < 0.001, ****p < 0.0001.

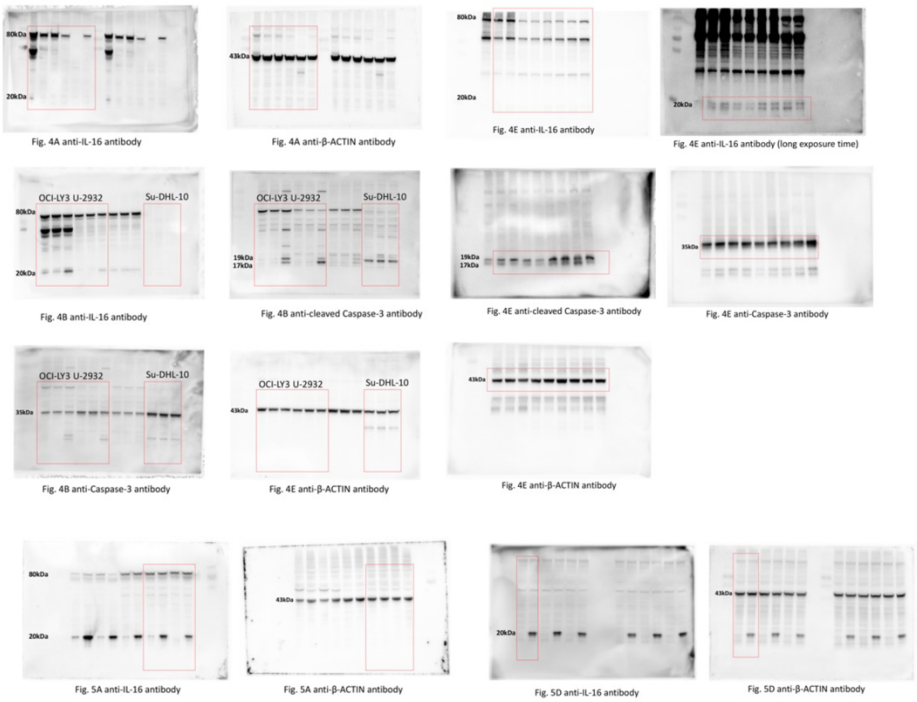

fig. S11. The original images of western blot image in the main article.